

# Combinatorial Bandit Bayesian Optimization for Tensor Outputs

Jingru Huang<sup>a</sup>, Haijie Xu<sup>a</sup>, Jie Guo<sup>b</sup>, Manrui Jiang<sup>a</sup>, Chen Zhang<sup>a</sup> \*

<sup>a</sup> Department of Industrial Engineering, Tsinghua University, Beijing 100084, China

<sup>b</sup> College of Economics and Management, Nanjing University of Aeronautics and Astronautics, Nanjing 211106, China

jingruhuang@tsinghua.edu.cn, xu-hj22@mails.tsinghua.edu.cn,  
guojie25@nuaa.edu.cn, jiangmanrui@mail.tsinghua.edu.cn,  
zhangchen01@tsinghua.edu.cn

## Abstract

Bayesian optimization (BO) has been widely used to optimize expensive and black-box functions across various domains. Existing BO methods have not addressed tensor-output functions. To fill this gap, we propose a novel tensor-output BO method. Specifically, we first introduce a tensor-output Gaussian process (TOGP) with two classes of tensor-output kernels as a surrogate model of the tensor-output function, which can effectively capture the structural dependencies within the tensor. Based on it, we develop an upper confidence bound (UCB) acquisition function to select the queried points. Furthermore, we introduce a more complex and practical problem setting, named combinatorial bandit Bayesian optimization (CBBO), where only a subset of the outputs can be selected to contribute to the objective function. To tackle this, we propose a tensor-output CBBO method, which extends TOGP to handle partially observed outputs, and accordingly design a novel combinatorial multi-arm bandit-UCB2 (CMAB-UCB2) criterion to sequentially select both the queried points and the optimal output subset. Theoretical regret bounds for the two methods are established, ensuring their sublinear performance. Extensive synthetic and real-world experiments demonstrate their superiority.

## 1 Introduction

Bayesian optimization (BO) is a widely used strategy for optimizing expensive, black-box objective functions (Frazier, 2018; Wang et al., 2023). Its effectiveness has led to successful applications in various domains such as hyperparameter tuning, experimental design, and robotics (Snoek et al., 2012; Shields et al., 2021; Wang et al., 2022). Most existing BO methods focus on scalar outputs (Bull, 2011; Wu et al., 2017), while some recent studies have extended BO to handle multi-output scenarios (Chowdhury & Gopalan, 2021; Tu et al., 2022; Maddox et al., 2021; Song et al., 2022). However, to the best of our knowledge, no prior work has addressed tensor-output BO, where the system output is a multi-mode tensor. In contrast, tensor-output data have been extensively explored in other areas, including tensor decomposition (Abed-Meraim et al., 2022), tensor regression (Lock, 2018), and tensor completion (Song et al., 2019), among others.

In current multi-output BO (MOBO) methods, a surrogate model, typically a multi-output Gaussian process (GP) or multiple scalar-output GPs, is constructed from observed data, and an acquisition function is used to sequentially select queried points by balancing exploration and exploitation. A straightforward approach to handling the tensor output is to vectorize it and apply existing MOBO methods. However, this neglects the intrinsic structural correlations within tensors, particularly the mode-wise dependencies that are critical in many applications. As a result, when optimizing the acquisition function to identify the

---

\*Corresponding author.

global optimum, MOBO methods may become less effective. As such, it is essential to construct a GP to directly model tensor structures. Existing tensor-output GP methods are based on full separable structures, where the joint covariance is decomposed into a Kronecker product of covariance matrices across each output mode and the input. (Kia et al., 2018; Zhe et al., 2019; Belyaev et al., 2015). While computationally attractive, such separability assumes that correlations across tensor modes are independent of the input, which is often unrealistic in complex real-world systems such as spatiotemporal processes (Hristopulos, 2023). This mismatch can lead to inaccurate modeling, numerical instability in posterior inference, and ultimately degraded BO performance. Therefore, in this paper, we first aim to construct a more flexible and scalable GP model that can capture input-dependent correlations within tensor outputs. Then, we aim to design an acquisition function and the sequential querying policy tailored for tensor-output BO.

Furthermore, we consider a more complex and practical setting in which only a subset of the tensor outputs can be selected to contribute to the objective function. This naturally transforms the problem into a combinatorial multi-armed bandit (CMAB) setting. Specifically, each tensor element is treated as an individual arm, and at each round, a subset of arms, referred to as a super-arm, is selected. The objective value associated with the chosen super-arm is then observed, which we interpret as the reward. We term this novel problem as combinatorial bandit Bayesian optimization (CBBO). The goal of CBBO with tensor outputs is to jointly identify the optimal input in the search space and the corresponding best super-arm over the tensor outputs. Recent studies have explored combining BO with multi-armed bandits (MAB), often referred to as bandit Bayesian optimization (BBO), to address mixed input spaces with both continuous and categorical variables (Nguyen et al., 2020; Ru et al., 2020; Huang et al., 2022). In such settings, categorical variables are viewed as tensor modes, with their categories corresponding to elements along each mode. Selecting one category per mode corresponds to choosing a single arm along each mode, which can be viewed as a special case of CBBO. However, existing BBO methods cannot be directly extended to the CBBO setting for two main reasons. First, they typically model the outputs associated with categorical variables using independent GPs, thereby failing to capture the rich structural correlations inherent in tensor outputs. Second, their selection strategies rely on multiple independent MABs (i.e., selecting one arm per mode independently), whereas CBBO requires joint selection of multiple correlated arms. Thus, these BBO methods have less potential to be extended to our CBBO framework.

To address the aforementioned challenges, we propose a novel tensor-output Bayesian optimization framework, named TOBO, together with its extension to the CBBO setting, named TOCBBO. Our main contributions are summarized as follows:

- We propose a tensor-output Gaussian process (TOGP) with two classes of tensor-output kernels that explicitly incorporate tensor structure by extending the linear model of coregionalization from vector-valued outputs to tensor-valued outputs. The proposed kernels capture rich dependencies across tensor modes and across the input domain.
- Using the TOGP model as a surrogate, we develop a TOBO framework based on the upper confidence bound (UCB) acquisition. We establish a sublinear regret bound for TOBO, which is the first regret analysis for tensor-valued outputs under a Bayesian framework.
- We formulate a novel problem setting, referred to as CBBO. To address this setting, we design the TOCBBO framework by introducing a CMAB-UCB2 acquisition function, which integrates the UCB criterion for input selection with the CMAB-UCB criterion for super-arm selection. We further establish a sublinear regret bound for TOCBBO.
- We demonstrate the efficiency and superiority of our methods through three synthetic experiments and four real-world applications.

Notably, compared to existing TOGP methods (Belyaev et al., 2015; Kia et al., 2018; Zhe et al., 2019), our model provides a more general kernel construction framework, as their tensor-output kernels correspond to specific choices of low-rank tensor decompositions, while

our LMC-based formulation allows arbitrary tensor constraints to be incorporated into the coregionalization matrix. Compared to existing BO methods (Srinivas et al., 2009; Belakaria et al., 2019; Chowdhury & Gopalan, 2021), our work is the first to establish a BO framework for tensor outputs and further extend it to the proposed CBBO setting. Moreover, our contributions lie in deriving regret bounds for both TOBO and TOCBBO based on concentration inequalities tailored to the proposed TOGP under the Bayesian framework.

## 2 Related works

**High-order Gaussian process (HOGP):** Existing studies for modeling HOGP rely on separable kernel structures. In particular, Belyaev et al. (2015) proposes a tensor-variate GP with separable covariance across tensor modes, Kia et al. (2018) develops a scalable multi-task GP for tensor outputs by factorizing the cross-covariance kernel into mode-wise and input components, and Zhe et al. (2019) introduces a scalable high-order GP framework based on Kronecker kernels. While such formulations simplify computation, they inherently assume that correlations across tensor modes are independent of the input, which limits their ability to capture input-dependent dependencies. Recent studies have studied non-separable kernel functions for multi-output GPs (MOGPs), including convolution emulator-based kernels (Fricker et al., 2013), linear model of coregionalization-based kernels (Fricker et al., 2013; Li & Zhou, 2016; Bruinsma et al., 2020), and linear damped harmonic oscillator-based kernels (Hristopulos, 2023). Another equivalent formulation for MOGP is called multi-task GPs, where each task corresponds to an element of the outputs (Yu et al., 2018; Chowdhury & Gopalan, 2021; Maddox et al., 2021). However, these approaches generally treat outputs as vectors and cannot exploit the inherent multi-mode structure of tensor data, see Section 1.

**Multi-output Bayesian optimization (MOBO):** MOBO typically refers to either multi-task BO or multi-objective BO (Frazier, 2018; Wang et al., 2023). A desirable property of BO algorithms is to be no-regret, i.e., achieving cumulative regret  $R(T) = o(T)$  after  $T$  rounds (Srinivas et al., 2009; Chowdhury & Gopalan, 2021). Recent works have proposed various MOBO methods with theoretically grounded acquisition functions. In particular, Chowdhury & Gopalan (2021); Dai et al. (2020); Sessa et al. (2023) employed UCB for multi-task BO and obtained  $O(\sqrt{T})$  regret. For multi-objective BO, Belakaria et al. (2019); Zhang et al. (2025) study multi-objective BO using max-value entropy search and achieved  $O(\sqrt{T})$  regret, and Daulton et al. (2022a) proposes a trust-region-based criterion with  $O(\sqrt{T} \log T)$  regret. In contrast, another class of MOBO methods focuses on empirical performance without regret guarantees, including improvement-based criteria (Uhrenholt & Jensen, 2019; Daulton et al., 2020; 2022b), entropy-based search criteria (Hernández-Lobato et al., 2014; 2016; Tu et al., 2022), and information gain-based approaches (Chowdhury & Gopalan, 2021). While effective in multi-output settings, these methods do not directly leverage the structured tensor correlations and are thus less suitable for our TOBO framework. Furthermore, hypervolume-based and entropy search-based multi-objective BO methods cannot be applied to tensor outputs because of their prohibitive computational complexity as the number of objectives grows.

**Bandit Bayesian optimization (BBO):** BBO combines BO with multi-armed bandit algorithms to handle optimization problems in mixed input spaces with both continuous and categorical variables. Nguyen et al. (2020); Huang et al. (2022) considers an optimization problem with one continuous and one categorical variable, integrating BO with MAB-Thompson sampling with  $\mathcal{O}(\sqrt{T^{\alpha+1}} \log T)$  regret. Ru et al. (2020) extends this idea to multiple categorical variables, introducing CoCaBO, by employing EXP3 (Auer et al., 2002) for categorical selection and achieving  $\mathcal{O}(\sqrt{T} \log T)$  regret. Although such settings can be regarded as special cases of CBBO, directly extending them is challenging due to the tensor-output structure and the need to jointly select multiple correlated arms.

In this section, we propose a novel tensor-output Bayesian optimization (TOBO) framework for optimizing systems with tensor-valued outputs. Let  $\mathbf{f} : \mathcal{X} \rightarrow \mathcal{Y}$  denote the black-box, expensive-to-evaluate function, where the input  $\mathbf{x} = (x_1, \dots, x_d)$  is a  $d$ -dimensional vector defined on a compact and convex region  $\mathcal{X} \subset \mathbb{R}^d$ , and the output  $\mathbf{f}(\mathbf{x}) \in \mathcal{Y} \subset \mathbb{R}^{t_1 \times \dots \times t_m}$

Table 1: Comparison of related works and our proposed method

Type	Literature	GP			BO (Regret)	BBO (Regret)	CBBO (Regret)
		Tensor structure	Separable (Independent modes)	Non-separable (Cross-mode correlations)			
HOGP	Belyaev et al. (2015) Kia et al. (2018) Zhe et al. (2019)	✓	✓	✗	✗	✗	✗
MOGP	Fricker et al. (2013) Li & Zhou (2016) Hristopulos (2023)	✗	✗	✓	✗	✗	✗
MTBO	Dai et al. (2020) Sessa et al. (2023)	✗	✓	✗	$\sqrt{(\mathcal{O}(\sqrt{T}))}$	✗	✗
MTBO	Chowdhury & Gopalan (2021)	✗	✓	✓	$\sqrt{(\mathcal{O}(\sqrt{T}))}$	✗	✗
MOBO	Belakaria et al. (2019) Zhang et al. (2025)	✗	✗	✗	$\sqrt{(\mathcal{O}(\sqrt{T}))}$	✗	✗
MOBO	Daulton et al. (2022a)	✗	✗	✗	$\sqrt{(\mathcal{O}(\sqrt{T} \log T))}$	✗	✗
BBO	Nguyen et al. (2020) Huang et al. (2022)	✗	✓	✗	$\sqrt{(\mathcal{O}(\sqrt{T^{\alpha+1}} \log T))}$	$\sqrt{(\mathcal{O}(\sqrt{T^{\alpha+1}} \log T))}$	✗
BBO	Ru et al. (2020)	✗	✓	✗	$\sqrt{(\mathcal{O}(\sqrt{T} \log T))}$	$\sqrt{(\mathcal{O}(\sqrt{T} \log T))}$	✗
TOBO+TOCBBO	Our proposed method	✓	✓	✓	$\sqrt{(\mathcal{O}(\sqrt{T} \log T))}$	$\sqrt{(\mathcal{O}(\sqrt{T} \log T))}$	$\sqrt{(\mathcal{O}(\sqrt{T} \log T))}$

is a tensor with  $m$  modes. Denote  $f_{i_1, \dots, i_m}(\mathbf{x})$  as the  $(i_1, \dots, i_m)$ -th entry of the tensor, where  $i_l = 1, \dots, t_l$  for  $l = 1, \dots, m$ , and let  $T = \prod_{l=1}^m t_l$  be the total number of elements. To optimize tensor-output systems, an intuitive way is to map the tensor-valued objective into a scalar function. To this end, we introduce a bounded linear operator  $L_f \in \mathcal{L}(\mathcal{Y}, \mathbb{R})$ , where  $\mathcal{L}(\mathcal{Y}, \mathbb{R})$  denotes the set of bounded linear operators from  $\mathcal{Y}$  to  $\mathbb{R}$ . The optimization problem is thus

$$\mathbf{x}^* = \arg \max_{\mathbf{x} \in \mathcal{X}} L_f \mathbf{f}(\mathbf{x}). \quad (1)$$

To solve this problem, the proposed TOBO aims to sequentially select inputs  $\mathbf{x}_i$  and observe the corresponding tensor outputs,

$$\mathbf{y}_i = \mathbf{f}(\mathbf{x}_i) + \boldsymbol{\varepsilon}_i, \quad \forall i = 1, 2, \dots \quad (2)$$

where  $\boldsymbol{\varepsilon}_i \in \mathbb{R}^{t_1 \times \dots \times t_m}$  denotes i.i.d. measurement noise with  $\text{vec}(\boldsymbol{\varepsilon}_i) \sim \mathcal{N}(0, \tau^2 \mathbf{I}_T)$ , and  $\text{vec} : \mathcal{Y} \rightarrow \mathbb{R}^T$  is the vectorization operator.

Based on the collected data, we construct a tensor-output Gaussian process (TOGP) with two classes of tensor-output kernels to model  $\mathbf{f}$ , as detailed in Subsection 3.1. Then, we develop a UCB-based acquisition strategy to efficiently identify the maximizer  $\mathbf{x}^*$ , as presented in Subsection 3.2.

### 3.1 Tensor-output Gaussian process

Define the prior of  $\mathbf{f} : \mathcal{X} \rightarrow \mathcal{Y}$  as a tensor-output Gaussian process (TOGP):

$$\text{vec}(\mathbf{f}(\mathbf{x})) \sim \mathcal{TOGP}(\boldsymbol{\mu}, \sigma^2 \mathbf{K}(\mathbf{x}, \mathbf{x}')), \quad \forall \mathbf{x}, \mathbf{x}' \in \mathcal{X}, \quad (3)$$

where  $\boldsymbol{\mu} \in \mathbb{R}^T$  is the prior mean,  $\sigma^2 > 0$  is a variance hyperparameter, and  $\mathbf{K}(\mathbf{x}, \mathbf{x}') \in \mathbb{R}^{T \times T}$  is a symmetric and positive semi-definite kernel function. The classes of  $\mathbf{K}(\mathbf{x}, \mathbf{x}')$  are discussed later.

Given  $n$  observations  $\mathbf{X}_n = (\mathbf{x}_1, \dots, \mathbf{x}_n)^\top$  and  $\mathbf{Y}_n = (\text{vec}(\mathbf{y}_1)^\top, \dots, \text{vec}(\mathbf{y}_n)^\top)^\top$ , the posterior of the vectorized  $\mathbf{f}$  at a new input  $\mathbf{x} \in \mathcal{X}$  is a  $T$ -dimensional Gaussian with mean and covariance,

$$\hat{\boldsymbol{\mu}}_n(\mathbf{x}) = \boldsymbol{\mu} + \mathbf{K}_n^\top(\mathbf{x}) (\mathbf{K}_n + \eta \mathbf{I}_{nT})^{-1} (\mathbf{Y}_n - \mathbf{1}_n \otimes \boldsymbol{\mu}), \quad (4)$$

$$\hat{\mathbf{K}}_n(\mathbf{x}, \mathbf{x}) = \sigma^2 \left[ \mathbf{K}(\mathbf{x}, \mathbf{x}) - \mathbf{K}_n^\top(\mathbf{x}) (\mathbf{K}_n + \eta \mathbf{I}_{nT})^{-1} \mathbf{K}_n(\mathbf{x}) \right], \quad (5)$$

where  $\mathbf{K}_n(\mathbf{x}) \in \mathbb{R}^{nT \times T}$  is the block column matrix with  $i$ -th block  $\mathbf{K}(\mathbf{x}_i, \mathbf{x})$ ,  $\mathbf{K}_n \in \mathbb{R}^{nT \times nT}$  is the block matrix with  $(i, j)$ -block  $\mathbf{K}(\mathbf{x}_i, \mathbf{x}_j)$ ,  $\mathbf{1}_n$  is the  $n$ -dimensional vector of ones, and  $\eta = \tau^2 / \sigma^2$ .

To specify the tensor-output kernel for TOGP, we introduce two classes of kernels. The first class is the non-separable tensor-output kernel. Specifically, any GP can be

represented as a convolution of white noise processes (Higdon, 2002). For a tensor-output system  $\mathbf{f}$  with GP prior, each element of  $\mathbf{f}$  can be expressed as  $f_{i_1, \dots, i_m}(\mathbf{x}) = \int_{\mathcal{X}} g_{i_1, \dots, i_m}(\mathbf{z} - \mathbf{x}) w_{i_1, \dots, i_m}(\mathbf{z}) d\mathbf{z}$ , where  $w_{i_1, \dots, i_m}(\mathbf{z})$  denotes an independent white noise process with zero mean and covariance  $k_{i_1, \dots, i_m}(\mathbf{z} - \mathbf{z}')$ . Inspired by the linear model of coregionalization (LMC) (Fricker et al., 2013; Li & Zhou, 2016), we consider a degenerate choice  $g_{i_1, \dots, i_m}(\mathbf{z} - \mathbf{x}) = \sum_{l=1}^m \sum_{j=1}^{t_l} A_l(i_1, \dots, i_m) \delta(\mathbf{z} - \mathbf{x})$ , so that  $f_{i_1, \dots, i_m}(\mathbf{x}) = \sum_{l=1}^m \sum_{j=1}^{t_l} A_l(i_1, \dots, i_m) w_{i_1, \dots, i_m}(\mathbf{x})$ , where  $A_l(i_1, \dots, i_m)$  denotes the  $(i_1, \dots, i_m)$ -th element of the tensor  $\mathbf{A}_l \in \mathbb{R}^{t_1 \times \dots \times t_m}$ . Expanding the LMC along tensor modes yields  $\mathbf{f}(\mathbf{x}) = \sum_{l=1}^m \sum_{j=1}^{t_l} \mathbf{A}_l \mathbf{w}(\mathbf{x})$  with zero mean and the covariance  $\text{Cov}(\text{vec}(\mathbf{f}(\mathbf{x})), \text{vec}(\mathbf{f}(\mathbf{x}')) = \sum_{l=1}^m \sum_{j=1}^{t_l} \text{vec}(\mathbf{A}_l) \text{vec}(\mathbf{A}_l)^\top k_{lj}(\mathbf{x}, \mathbf{x}')$ . The non-separable tensor-output kernel is defined as

Definition 1. Define the non-separable tensor-output kernel  $\mathbf{K}(\mathbf{x}, \mathbf{x}')$  for any  $\mathbf{x}, \mathbf{x}' \in \mathcal{X}$ :

$$\mathbf{K}(\mathbf{x}, \mathbf{x}') = \sum_{l=1}^m \sum_{j=1}^{t_l} \text{vec}(\mathbf{A}_l) \text{vec}(\mathbf{A}_l)^\top k_{lj}(\mathbf{x}, \mathbf{x}'), \quad (6)$$

where  $\mathbf{A}_l \in \mathbb{R}^{t_1 \times \dots \times t_m}$  is a core tensor and  $k_{lj}(\mathbf{x}, \mathbf{x}')$  are base kernels (e.g., Matérn or Gaussian) on  $\mathcal{X}$ . This construction induces correlations both across and within tensor modes that vary with the input, thus yielding a non-separable covariance structure.

Furthermore, if all  $w_{i_1, \dots, i_m}(\mathbf{z})$  share the same covariance  $k(\mathbf{z}, \mathbf{z}')$  for  $i_l \in [t_l]$ ,  $l = 1, \dots, m$ , and the convolution degenerates to  $g_{i_1, \dots, i_m}(\mathbf{z}) = A_{i_1, \dots, i_m} \delta(\mathbf{z} - \mathbf{x})$ , then the induced tensor-output kernel reduces to a separable structure as

Definition 2. Define the separable tensor-output kernel  $\mathbf{K}(\mathbf{x}, \mathbf{x}')$  for any  $\mathbf{x}, \mathbf{x}' \in \mathcal{X}$ :

$$\mathbf{K}(\mathbf{x}, \mathbf{x}') = \text{vec}(\mathbf{A}) \text{vec}(\mathbf{A})^\top k(\mathbf{x}, \mathbf{x}'). \quad (7)$$

where  $\mathbf{A} \in \mathbb{R}^{t_1 \times \dots \times t_m}$  is a core tensor, and  $k(\cdot, \cdot)$  is a base kernel on  $\mathcal{X}$ . This structure yields a separable kernel in which the correlations across tensor modes are independent of the input.

Note that  $\mathbf{K}(\mathbf{x}, \mathbf{x}')$  is designed to capture both the correlation across inputs and the correlation within the tensor output. For the non-separable tensor-output kernel in (6), the base kernel  $k_{lj}(\mathbf{x}, \mathbf{x}')$  models the covariance between the inputs  $\mathbf{x}$  and  $\mathbf{x}'$ , while the matrix  $\text{vec}(\mathbf{A}_l) \text{vec}(\mathbf{A}_l)^\top$  describes the covariance structure among the elements of the output tensor. For the separable tensor output kernel in (7),  $k(\mathbf{x}, \mathbf{x}')$  captures the input correlation, and  $\text{vec}(\mathbf{A}) \text{vec}(\mathbf{A})^\top$  specifies the mode-wise covariance structure within the tensor output.

Proposition 1. The kernel function  $\mathbf{K}$  in Definitions 1–2 for the TOGP is symmetric and positive semi-definite on  $\mathcal{X}$ . Specifically: (1)  $\forall \mathbf{x}, \mathbf{x}' \in \mathcal{X}$ , the kernel satisfies symmetry:  $\mathbf{K}(\mathbf{x}, \mathbf{x}') = \mathbf{K}(\mathbf{x}', \mathbf{x})^\top$ ; (2)  $\forall \mathbf{y}_1, \dots, \mathbf{y}_n \in \mathcal{Y}$ , the Gram matrix is positive semi-definite:  $\sum_{i,j=1}^n \text{vec}(\mathbf{y}_i)^\top \mathbf{K}(\mathbf{x}_i, \mathbf{x}_j) \text{vec}(\mathbf{y}_j) \geq 0$ .

Its proof is given in Appendix E. Proposition 1 thus ensures that two classes of tensor-output kernels yield valid covariance kernels for TOGP, ensuring that the induced TOGP is well defined.

Remark 1. For the core tensors  $\{\mathbf{A}_l\}_{l=1}^m$  in (6) and  $\mathbf{A}$  in (7), there are  $mT$  and  $T$  parameters to be estimated, respectively. To reduce the complexity, some low-rank decomposition-based structures can be applied to core tensors, such as CANDECOMP/PARAFAC (CP) decomposition (Goulart et al., 2015) and tensor-train (TT) decomposition (Oseledets, 2011). Details are shown in Appendix B.

Denote the hyperparameters as  $\Theta = \{\theta, \mathbf{a}, \sigma^2, \tau^2\}$ . For the kernel in (6),  $\theta = \{\theta_{l,j}\}_{l,j=1}^{m,t_l}$  are the scale parameters of the base kernels  $\{k_{l,j}\}$ , and  $\mathbf{a} = \{a_{lj}\}_{l,i,j}^{m,m,t_l}$  are the parameters of  $\{\mathbf{A}_l\}_{l=1}^m$ . For the kernel in (7),  $\theta = \{\theta_1, \dots, \theta_d\}$  is the scale parameters of  $k$ , and  $\mathbf{a} = \{a_{ij}\}_{i,j}^{m,t_l}$  are the parameters of  $\mathbf{A}$ . The hyperparameters  $\Theta$  are estimated via maximum likelihood. The detailed estimation, algorithm, and complexity analysis are provided in Appendix C.

Remark 2. The ranks of the core tensors  $\mathbf{A}_l$  in the proposed TOGP model are chosen via cross-validation for  $l = 1, \dots, m$ . Let  $\mathbf{R}_c = \{\mathbf{r}_1, \dots, \mathbf{r}_c\}$  be the set of candidate ranks, we fit the TOGP model and evaluate its predictive accuracy on a held-out validation set using the mean absolute error (MAE) criterion. The selected rank is given by  $\mathbf{r}^* = \arg \min_{\mathbf{r} \in \mathbf{R}_c} \text{MAE}(\mathbf{r})$ , where  $\text{MAE}(\mathbf{r}) = \frac{1}{n_{\text{test}}} \sum_{i=1}^{n_{\text{test}}} \left\| \frac{\mathbf{f}_i - \hat{\mathbf{f}}_i(\mathbf{r})}{\mathbf{f}_i} \right\|$ . The data-driven selection balances model flexibility and complexity, thereby mitigating overfitting while preserving expressive capacity.

Remark 3. To improve scalability for large tensor outputs, we adopt a Nyström low-rank approximation strategy. Specifically, based on data  $\mathbf{X}_n$  and  $\mathbf{Y}_n$ , consider the spectral decomposition  $\mathbf{K}_n = \mathbf{U}_n \mathbf{\Lambda}_n \mathbf{U}_n^\top$ , where  $\mathbf{\Lambda}_n = \text{diag}(\lambda_1, \lambda_2, \dots, \lambda_{nT})$  denotes eigenvalues ordered as  $\lambda_1 \geq \lambda_2 \geq \dots \geq \lambda_{nT} > 0$ . We approximate  $\mathbf{K}_n$  using the leading  $l$  ( $\ll nT$ ) eigenpairs, that is,  $\mathbf{K}_n \approx \mathbf{U}_l \mathbf{\Lambda}_l \mathbf{U}_l^\top$ , where  $\mathbf{U}_l \in \mathbb{R}^{nT \times l}$  contains the first  $l$  eigenvectors and  $\mathbf{\Lambda}_l = \text{diag}(\lambda_1, \dots, \lambda_l)$ . The rank  $l$  is selected by cumulative explained variance:  $l = \min_{l_0} \left\{ l_0 \in \{1, \dots, nT\} : \sum_{i=1}^{l_0} \lambda_i / \sum_{i=1}^{nT} \lambda_i \geq c \right\}$ . The Nyström method approximates  $\mathbf{K}_n$  by selecting  $n_l$  ( $\ll nT$ ) landmark columns and extending a small eigendecomposition, which yields a computational cost of evaluating  $(\mathbf{K}_n + \eta \mathbf{I}_{nT})^{-1}$  as  $\mathcal{O}(nTn_l^2 + n_l^3)$  (Williams & Seeger, 2000). Thus, the overall computational complexity for training TOGP becomes  $\mathcal{O}((nTn_l^2 + n_l^3 + n^2T^2m_h) \log n)$ .

### 3.2 Upper Confidence Bound Acquisition Strategy

Building on the proposed TOGP as a surrogate for  $\mathbf{f}$ , we now develop a UCB-based acquisition strategy. At round  $n + 1$ , given past observations  $\mathbf{X}_n$  and  $\mathbf{Y}_n$ , we update the hyperparameters  $\Theta_n$  as well as the posterior mean (4) and covariance (5) of  $\mathbf{f}$ . The UCB acquisition function for the scalarization-based objective in (1) is defined as

$$\alpha_{UCB}(\mathbf{x} \mid \mathcal{D}_n) = L_f \hat{\mathbf{\mu}}_n(\mathbf{x}) + \beta_n \|\hat{\mathbf{K}}_n(\mathbf{x}, \mathbf{x})\|^{1/2}, \quad (8)$$

where  $\beta_n > 0$  is a tuning parameter that balances exploration and exploitation. This criterion encourages exploration in directions with greater predictive uncertainty under the tensor-output setting. The next query is then selected by maximizing (8):

$$\mathbf{x}_{n+1} = \arg \max_{\mathbf{x} \in \mathcal{X}} \alpha_{UCB}(\mathbf{x} \mid \mathcal{D}_n). \quad (9)$$

The complete TOBO algorithm and its complexity analysis are given in Appendix D.

We now analyze the theoretical properties of the TOBO method under specific conditions. To this end, we first introduce the following definition for two commonly used regrets.

Definition 3. At each round  $n$ , the TOBO method selects a queried input  $\mathbf{x}_n \in \mathcal{X}$ . The instantaneous regret is defined as  $r_n = L_f \mathbf{f}(\mathbf{x}^*) - L_f \mathbf{f}(\mathbf{x}_n)$ , and the cumulative regret up to round  $N$  is defined as  $R_N = \sum_{n=1}^N [L_f \mathbf{f}(\mathbf{x}^*) - L_f \mathbf{f}(\mathbf{x}_n)]$ .

The regret quantifies the gap from not knowing the objective in advance. A good strategy can achieve a sub-linear cumulative regret so that the average regret per round converges to zero as  $N \rightarrow \infty$ .

Assumption 1. Assume that the true system  $\mathbf{f}$  is a TOGP with kernel  $\mathbf{K}$  as defined in (6)–(7).

Assumption 2. The scalarization operator  $L_f$  in (1) is  $L$ -Lipschitz with respect to  $\mathbf{f}$  under the  $l_2$  norm, i.e., for any  $\mathbf{x}_i, \mathbf{x}_j \in \mathcal{X}$ ,  $|L_f(\mathbf{f}(\mathbf{x}_i)) - L_f(\mathbf{f}(\mathbf{x}_j))| \leq L \|\mathbf{f}(\mathbf{x}_i) - \mathbf{f}(\mathbf{x}_j)\|$  holds.

Assumption 1 ensures that the objective function  $\mathbf{f}$  is a TOGP, which is a basic setting under the Bayesian framework. Assumption 2 demonstrates that the scalarization-based objective is stable under small perturbations of the input.

Lemma 1. Let  $\partial \text{vec}(\mathbf{f}) / \partial x_j \in \mathbb{R}^T$  be the gradient of  $\text{vec}(\mathbf{f})$  with respect to the  $j$ -th coordinate of  $\mathbf{x} \in \mathcal{X}$ . Then,  $\partial \text{vec}(\mathbf{f}) / \partial x_j$  is a GP with covariance  $\mathbf{K}^\nabla(x_j, x'_j)$ . Under Assumptions 1, given data  $\mathbf{X}_n$  and  $\mathbf{Y}_n$  with  $n \geq 1$ , there exist constants  $a, b > 0$  such that

$$\Pr \left( \sup_{\mathbf{x} \in \mathcal{X}} \|\partial \text{vec}(\mathbf{f}) / \partial x_j\| > L' + C_\nabla \right) \leq a \exp(-L'^2/b^2), \quad j = 1, \dots, d. \quad (10)$$

where  $C_\nabla = \sup_{\mathbf{x} \in \mathcal{X}} \sqrt{\text{tr}(\hat{\mathbf{K}}_n^\nabla(x_j, x_j))}$  and  $L' > 0$ .

Its proof is given in Appendix F. Lemma 1 shows that the derivative of the vectorized TOGP remains Gaussian and holds high-probability confidence bounds.

**Theorem 1.** Under Assumptions 1–2, define  $C_n = \sup_{\mathbf{x} \in \mathcal{X}} \text{tr}(\hat{\mathbf{K}}_n(\mathbf{x}, \mathbf{x}))/\lambda_{\max}^{(n)}(\mathbf{x})$ , where  $\lambda_{\max}^{(n)}(\mathbf{x})$  is the largest eigenvalue of  $\hat{\mathbf{K}}_n(\mathbf{x}, \mathbf{x})$ . Suppose  $\mathcal{X} \subseteq [0, r]^d$ . Then for any  $\delta \in (0, 1)$ , the TOBO method with  $\beta_n = \sqrt{C_n} + 2d \log(rdn^2(b\sqrt{\log(da/\delta)} + C_\nabla)/\delta)$  holds that,  $\Pr(R_N \leq L \left( \sqrt{C_1 N \gamma_N(\mathbf{K}, \eta)} \beta_N + \frac{\pi^2}{6} \right)) \geq 1 - \delta$ , where  $\gamma_N(\mathbf{K}, \eta) := \max_{\mathcal{X}_N \subset \mathcal{X}} \frac{1}{2} \log \det(\mathbf{I}_{NT} + \eta^{-1} \mathbf{K}_N)$  denotes the maximum information gain, and  $C_1 > 0$  is a constant.

Its proof is given in Appendix G. Theorem 1 establishes that the cumulative regret of TOBO is sub-linear with high probability.

**Proposition 2.** If  $\mathbf{K}(\mathbf{x}, \mathbf{x}')$  is specified as the separable kernel in Definition 2, then the maximum information gain satisfies  $\gamma_n(\mathbf{K}, \eta) = \mathcal{O}(T \log(n)^{d+1})$  when  $k(\mathbf{x}, \mathbf{x}')$  is a Gaussian kernel, and  $\gamma_n(\mathbf{K}, \eta) = \mathcal{O}(T n^{d(d+1)/(2\nu+d(d+1))} \log(n))$  when  $k(\mathbf{x}, \mathbf{x}')$  is a Matérn kernel with smoothness parameter  $\nu > 1$ . Details of the analysis are provided in Appendix H.

## 4 Tensor-output combinatorial bandit Bayesian optimization

We now consider a more challenging optimization problem in which only  $k < T$  elements of the tensor output can contribute to the objective function. Formally, we define  $\tilde{\mathbf{f}}(\mathbf{x}, \boldsymbol{\lambda}) = \mathbf{e}(\boldsymbol{\lambda}) \text{vec}(\mathbf{f}(\mathbf{x})) \in \tilde{\mathcal{Y}}$ , where  $\boldsymbol{\lambda} = (\lambda_1, \dots, \lambda_T)^\top$  is a binary indicator vector in  $\Lambda = \{\boldsymbol{\lambda} \in \{0, 1\}^T : \mathbf{1}_n^\top \boldsymbol{\lambda} = k\}$  and  $\mathbf{e}(\boldsymbol{\lambda}) \in \{0, 1\}^{k \times T}$  is a binary selection matrix whose  $j$ -th row selects the  $i_j$ -th coordinate of  $\text{vec}(\mathbf{f}(\mathbf{x}))$ . The goal is to jointly identify the optimal input  $\mathbf{x}^* \in \mathcal{X}$  and the optimal subset of  $k$  elements, represented by a binary vector  $\boldsymbol{\lambda}^* \in \Lambda$ , that maximize

$$(\mathbf{x}^*, \boldsymbol{\lambda}^*) = \arg \max_{\mathbf{x} \in \mathcal{X}, \boldsymbol{\lambda} \in \Lambda} H_f \tilde{\mathbf{f}}(\mathbf{x}, \boldsymbol{\lambda}), \quad (11)$$

where  $H_f$  is a bounded linear operator  $H_f \in \mathcal{L}(\tilde{\mathcal{Y}}, \mathbb{R})$ . By interpreting each tensor element as an individual arm, the selected subset of  $k$  elements corresponds to a super-arm  $\mathcal{S}$ , with  $j \in \mathcal{S}$  if  $\lambda_j = 1$  and  $j \notin \mathcal{S}$  otherwise. At each round  $i \in [N]$ , the learner selects an input  $\mathbf{x}_i$  and a super-arm  $\mathcal{S}_i = \{i_1, \dots, i_k\}$  of size  $k$ , equivalently encoded by  $\boldsymbol{\lambda}_i \in \Lambda$ . The observed output is a partial tensor  $\tilde{\mathbf{y}}_i \in \mathbb{R}^k$  indexed by  $\mathcal{S}_i$ , while outputs for unselected elements  $j \notin \mathcal{S}_i$  remain unobserved.

In this section, we propose a novel tensor-output combinatorial bandit Bayesian optimization (TOCBBO) framework to solve the above problem. In Subsection 4.1, we extend the TOGP model for partially observed outputs. In Subsection 4.2, we develop an efficient CMAB-UCB2 acquisition strategy that combines UCB for input selection with CMAB-UCB for super-arm selection.

### 4.1 Partially observed tensor-output Gaussian process

From the proposed TOGP in (3), the prior of  $\tilde{\mathbf{f}} : \mathcal{X} \times \Lambda \rightarrow \tilde{\mathcal{Y}}$  is a partially observed TOGP (PTOGP):

$$\tilde{\mathbf{f}}(\mathbf{x}, \boldsymbol{\lambda}) \sim \mathcal{PTOGP}(\mathbf{e}(\boldsymbol{\lambda})\boldsymbol{\mu}(\mathbf{x}), \tau^2 \mathbf{e}(\boldsymbol{\lambda})\mathbf{K}(\mathbf{x}, \mathbf{x}')\mathbf{e}(\boldsymbol{\lambda}')^\top), \quad \forall \mathbf{x}, \mathbf{x}' \in \mathcal{X}, \boldsymbol{\lambda}, \boldsymbol{\lambda}' \in \Lambda. \quad (12)$$

Let  $\mathbf{X}_n = (\mathbf{x}_1, \dots, \mathbf{x}_n)^\top$ ,  $\boldsymbol{\lambda}_n = (\lambda_1, \dots, \lambda_n)^\top$ , and  $\tilde{\mathbf{Y}}_n = (\tilde{\mathbf{y}}_1, \dots, \tilde{\mathbf{y}}_n)^\top$  be  $n$  partial observations, where  $\boldsymbol{\lambda}_i$  corresponds to the selected super-arm  $\mathcal{S}_i$ , and  $\tilde{\mathbf{y}}_i = \tilde{\mathbf{f}}(\mathbf{x}_i, \boldsymbol{\lambda}_i) + \tilde{\boldsymbol{\varepsilon}}_i$  with  $\tilde{\boldsymbol{\varepsilon}}_i \stackrel{\text{i.i.d.}}{\sim} \mathcal{N}(\boldsymbol{\mu}, \tau^2 \mathbf{I}_k)$ . Then, for a new input  $\mathbf{x}$  and a super-arm  $\mathcal{S}$  with indicator vector  $\boldsymbol{\lambda}$ , the posterior distribution of  $\tilde{\mathbf{f}}$  is a  $k$ -dimensional Gaussian with mean and covariance

$$\tilde{\boldsymbol{\mu}}_n(\mathbf{x}, \boldsymbol{\lambda}) = \mathbf{e}(\boldsymbol{\lambda})\boldsymbol{\mu}(\mathbf{x}) + \sigma^2 \mathbf{e}(\boldsymbol{\lambda})\mathbf{K}_n^\top(\mathbf{x})\mathbf{E}_n^\top \tilde{\boldsymbol{\Sigma}}_n^{-1} \left( \text{vec}(\tilde{\mathbf{Y}}_n) - \mathbf{E}_n(\mathbf{1}_n \otimes \boldsymbol{\mu}) \right), \quad (13)$$

$$\tilde{\mathbf{K}}_n(\mathbf{x}, \mathbf{x}'; \boldsymbol{\lambda}, \boldsymbol{\lambda}') = \sigma^2 [\mathbf{e}(\boldsymbol{\lambda})\mathbf{K}(\mathbf{x}, \mathbf{x}')\mathbf{e}(\boldsymbol{\lambda}')^\top - \sigma^2 \mathbf{e}(\boldsymbol{\lambda})\mathbf{K}_n^\top(\mathbf{x})\mathbf{E}_n \tilde{\boldsymbol{\Sigma}}_n^{-1} \mathbf{E}_n^\top \mathbf{K}_n(\mathbf{x}')\mathbf{e}(\boldsymbol{\lambda}')^\top], \quad (14)$$

where  $\tilde{\Sigma}_n = \sigma^2 \mathbf{E}_n \mathbf{K}_n \mathbf{E}_n^\top + \tau^2 \mathbf{I}_{nk}$ , and  $\mathbf{E}_n \in \mathbb{R}^{nk \times nT}$  is a  $n \times n$  block-diagonal matrix with the  $i$ -block given by  $\mathbf{e}(\boldsymbol{\lambda}_i)$ . It is easy to verify that the posterior covariance remains positive definite and symmetric. For hyperparameter estimation, we also employ the maximum likelihood estimation (MLE) framework for training the PTOGP. The detailed estimation, algorithm, and complexity analysis are presented in Appendix C.

#### 4.2 CMAB-UCB2 Acquisition Strategy

Building on the PTOGP, we now develop the TOCBBO method to sequentially select queried inputs  $\{\mathbf{x}_1, \dots, \mathbf{x}_N\}$  together with their associated super-arm indicators  $\{\boldsymbol{\lambda}_1, \dots, \boldsymbol{\lambda}_N\}$ . Directly optimizing (11) over both  $\mathbf{x}$  and  $\boldsymbol{\lambda}$  is computationally intractable, since identifying the optimal super-arm of size  $k$  from  $T$  arms requires a combinatorial search over  $\binom{T}{k}$  possible configurations. When coupled with the continuous optimization over  $\mathcal{X}$ , this joint problem becomes computationally prohibitive. To overcome this challenge, we propose a CMAB-UCB2 criterion that decomposes the optimization into two sequential steps.

At round  $n+1$ , let  $\mathbf{x}_n^*$  and  $\boldsymbol{\lambda}_n^*$  denote the best input and super-arm identified from the previous  $n$  rounds, that is,  $\{\mathbf{x}_n^*, \boldsymbol{\lambda}_n^*\} = \arg \max_{\{\mathbf{x}_i, \boldsymbol{\lambda}_i\}, i=1, \dots, n} H_f \tilde{\mathbf{f}}(\mathbf{x}_i, \boldsymbol{\lambda}_i)$ . In the first step, we fix the super-arm to  $\boldsymbol{\lambda}_n^*$  and query the next input by maximizing the UCB acquisition function conditioned on the fixed super-arm, i.e.,

$$\mathbf{x}_{n+1} = \arg \max_{\mathbf{x} \in \mathcal{X}} H_f \tilde{\mathbf{u}}_n(\mathbf{x}, \boldsymbol{\lambda}_n^*) + \tilde{\beta}_n \|\tilde{\mathbf{K}}_n(\mathbf{x}, \mathbf{x}; \boldsymbol{\lambda}_n^*, \boldsymbol{\lambda}_n^*)\|^{1/2}. \quad (15)$$

In the second step, given the chosen input  $\mathbf{x}_{n+1}$ , the optimization problem for selecting  $\boldsymbol{\lambda}_{n+1}$  reduces to a CMAB problem. To this end, we adopt the CMAB-UCB criterion by constructing a UCB for each super-arm and selecting the one that maximizes the sum of the upper confidence value:

$$\boldsymbol{\lambda}_{n+1} = \arg \max_{\boldsymbol{\lambda} \in \Lambda} H_f \tilde{\mathbf{u}}_n(\mathbf{x}_{n+1}, \boldsymbol{\lambda}) + \tilde{\rho}_n \|\tilde{\mathbf{K}}_n(\mathbf{x}_{n+1}, \mathbf{x}_{n+1}; \boldsymbol{\lambda}, \boldsymbol{\lambda})\|^{1/2}. \quad (16)$$

Here,  $\tilde{\beta}_n$  and  $\tilde{\rho}_n$  are tuning parameters controlling the trade-off between exploration and exploitation. The compute TOCBBO algorithm and its computational complexity analysis are provided in Appendix D.

We further analyze the regret bound of the TOCBBO method under specific conditions. The regret for CBBO is defined as follows:

**Definition 4.** At each round  $n$ , the TOCBBO method selects a queried input  $\mathbf{x}_n \in \mathcal{X}$  and a super arm  $\mathcal{S}_n$  with indicator  $\boldsymbol{\lambda}_n \in \Lambda$ . The instantaneous regret is defined as  $r_n = H_f \tilde{\mathbf{f}}(\mathbf{x}^*, \boldsymbol{\lambda}^*) - H_f \tilde{\mathbf{f}}(\mathbf{x}_n, \boldsymbol{\lambda}_n)$ , and the cumulative regret up to round  $N$  is defined as  $R_N = \sum_{n=1}^N [H_f \tilde{\mathbf{f}}(\mathbf{x}^*, \boldsymbol{\lambda}^*) - H_f \tilde{\mathbf{f}}(\mathbf{x}_n, \boldsymbol{\lambda}_n)]$ .

**Assumption 3.** The operator  $H_f$  in (11) is  $H$ -Lipschitz with respect to  $\tilde{\mathbf{f}}$  under the  $l_2$  norm, i.e., for  $\forall \mathbf{x}_i, \mathbf{x}_j \in \mathcal{X}$  and  $\boldsymbol{\lambda}_i, \boldsymbol{\lambda}_j \in \Lambda$ ,  $|H_f \tilde{\mathbf{f}}(\mathbf{x}_i, \boldsymbol{\lambda}_i) - H_f \tilde{\mathbf{f}}(\mathbf{x}_j, \boldsymbol{\lambda}_j)| \leq H \|\tilde{\mathbf{f}}(\mathbf{x}_i, \boldsymbol{\lambda}_i) - \tilde{\mathbf{f}}(\mathbf{x}_j, \boldsymbol{\lambda}_j)\|$  holds.

Assumption 3 ensures that  $H_f \tilde{\mathbf{f}}$  varies smoothly to changes for partially observed tensor outputs.

**Theorem 2.** Under Assumption 1 and Assumption 2, denote  $\tilde{C}_n = \sup_{\mathbf{x} \in \mathcal{X}} \frac{\text{tr}(\tilde{\mathbf{K}}_n(\mathbf{x}, \mathbf{x}; \boldsymbol{\lambda}_n^*, \boldsymbol{\lambda}_n^*))}{\lambda_{\max}^{(n)}(\mathbf{x}, \boldsymbol{\lambda}_n^*)}$ , where  $\lambda_{\max}^{(n)}(\mathbf{x}, \boldsymbol{\lambda}_n^*)$  is the largest eigenvalue of  $\tilde{\mathbf{K}}_n(\mathbf{x}, \mathbf{x}; \boldsymbol{\lambda}_n^*, \boldsymbol{\lambda}_n^*)$ . For any  $\delta \in (0, 1)$  and  $\eta > 0$ , the TOCBBO method with  $\tilde{\beta}_n = \sqrt{\tilde{C}_n} + 2d \log(\frac{rdn^2(b\sqrt{\log(da/\delta)} + \tilde{C}_n)}{l}\delta)$  and  $\tilde{\rho}_n = \sqrt{2 \log(\frac{NT\pi_n}{\delta})}$  holds that,  $\Pr\left(R_N \leq H \left(\sqrt{C_3 N \gamma_N(\tilde{\mathbf{K}}, \eta)} \tilde{\beta}_N + \frac{\pi^2}{6} + \sqrt{C_4 T N \tilde{\gamma}_N(\tilde{\mathbf{K}}, \eta)} \tilde{\rho}_N\right)\right) \geq 1 - \delta$ , where  $\gamma_n(\tilde{\mathbf{K}}, \eta) = \max_{\mathbf{X}_N \subset \mathcal{X}} \frac{1}{2} \log \det(\mathbf{I}_{kN} + \eta^{-1} \mathbf{E}_N \mathbf{K}_N \mathbf{E}_N^\top)$  is the maximum information gain

for inputs,  $\tilde{\gamma}_N(\tilde{\mathbf{K}}, \eta) = \max_{\mathbf{A}_N \subset \Lambda} \frac{1}{2} \log \det (\mathbf{I}_{kN} + \eta^{-1} \mathbf{E}_N \mathbf{K}_N \mathbf{E}_N^\top)$  is the maximum information gain for super-arms,  $\pi_n > 0$  is a sequence such that  $\sum_{l=1}^{\infty} 1/\pi_l = 1$ , and  $C_3, C_4 > 0$  are constants.

Its detailed proof is provided in I. Theorem 2 shows that the upper bound on the regret for the TOCBBO method is sublinear with a high probability.

**Proposition 3.** Suppose the kernel  $\mathbf{K}(\mathbf{x}, \mathbf{x}')$  follows the separable structure specified in Definition 2. The maximum information gain  $\gamma_n(\tilde{\mathbf{K}}, \eta)$  and  $\tilde{\gamma}_n(\tilde{\mathbf{K}}, \eta)$  are  $\mathcal{O}(T(\log n)^{d+1})$  and  $\mathcal{O}\left(Tn^{\frac{d(d+1)}{2\nu+d(d+1)}} \log n\right)$  for the Gaussian kernel and the Matérn kernel ( $\nu > 1$ ), respectively, where  $d$  denotes the input dimension. Details of the analysis are provided in Appendix J.

## 5 Experiments

We evaluate the performance of TOBO and TOCBBO using both synthetic and real-case data, and compare them with several baselines where the tensor output is vectorized and MOGPs are used as surrogate models. Specifically, we consider three GPs in the literature: (1) sMTGP: the scalable multi-task GP Kia et al. (2018); (2) MLGP: the multi-linear GP Yu et al. (2018); and (3) MVGP: the multi-variate GP Chen et al. (2020). For each GP, we examine two sequential BO sampling strategies: (1) the UCB criterion and (2) random sampling. In addition, we replace the UCB acquisition in TOBO and TOCBBO with random sampling to construct an ablation baseline, denoted as TOGP-RS. Detailed descriptions of all baseline settings are provided in Appendix K.

### 5.1 Synthetic experiments

We assume the true  $\mathbf{f}(\mathbf{x})$  takes the form  $\mathbf{f}(\mathbf{x}) = \mathbf{B} \otimes_1 \mathbf{U}_1 \otimes_2 \dots \otimes_{m-1} \mathbf{U}_{m-1} \otimes_m \mathbf{g}(\mathbf{x})$ , where each element of  $\mathbf{B} \in \mathbb{R}^{P_1 \times \dots \times P_m}$  is independently sampled from  $U(0, 1)$ , the  $ij$ -th element of  $\mathbf{U}_l \in \mathbb{R}^{P_l \times T_l}$  is defined as  $li \cos(ijl/2) + \sin(li)$ , and  $\mathbf{g}(\mathbf{x}) = (\sin(5\mathbf{x}), \cos(\mathbf{x})) \in \mathbb{R}^{P_m \times T_m}$ . Here  $P_m = d$  and  $\mathbf{x} \in [0, 1]^d$ . We consider three parameter settings for generating  $\mathbf{f}(\mathbf{x})$ : (1)  $m = 3$ ,  $(T_1, T_2, T_3) = (2, 4, 2)$ ,  $(P_1, P_2, P_3) = (3, 3, 3)$ ; (2)  $m = 2$ ,  $(T_1, T_2) = (3, 2)$ ,  $(P_1, P_2) = (3, 2)$ ; and (3)  $m = 3$ ,  $(T_1, T_2, T_3) = (4, 5, 2)$ ,  $(P_1, P_2, P_3) = (3, 3, 3)$ . The observations are collected as  $\mathbf{y}_i = \mathbf{f}(\mathbf{x}_i) + \boldsymbol{\varepsilon}_i$ , where  $\boldsymbol{\varepsilon}_i \stackrel{\text{i.i.d.}}{\sim} N(0, 0.1^2 \mathbf{I})$ . For CBBO tasks, we set  $k = T/6$ .

We generate  $n_{\text{train}} = 10d$  training samples and  $n_{\text{test}} = 5d$  testing samples using a Latin hypercube design (Santner et al., 2003). The training samples are used to estimate hyperparameters, and predictive performance is evaluated on the testing data in terms of NLL, MAE, and  $\|\text{Cov}\|$ , with detailed definitions provided in Appendix K. To balance modeling flexibility and computational complexity, we use the separable tensor-output kernel in (7) in Settings (1) and (2), and employ the non-separable tensor-output kernel in (6) in Setting (3). The results are summarized in Table 2. As shown, our proposed method achieves the

Table 2: The prediction performance of GPs in the three synthetic settings.

	Setting (1)			Setting (2)			Setting (3)		
	NLL	MAE	$\ \text{Cov}\ $	NLL	MAE	$\ \text{Cov}\ $	NLL	MAE	$\ \text{Cov}\ $
TOGP	503.0	0.1571	2.02	-18.1	0.1052	0.04	-3923.1	0.1372	2.82
sMTGP	749.4	0.1684	1.44	-5.0	0.1566	0.06	-3743.0	0.1501	22.01
MLGP	707937.1	0.9428	67.00	7066.9	0.8789	5.12	-55800.7	1.1670	0.06
MVGP	11152.2	0.6746	22.20	46.54	0.1784	0.10	-2583.1	1.0000	142.72

lowest NLL and MAE, indicating that the TOGP model provides the highest prediction accuracy. Among the three baselines, MLGP performs the worst because its covariance matrix is singular in this setting, which is more suitable for multi-task learning with varying sample sizes across tasks. sMTGP outperforms MVGP because sMTGP considers modeling each mode of the tensor output, and MVGP ignores the tensor structure by vectorizing it into a vector.

Table 3 summarizes the optimization performance of different methods for the BO and CBBO problems. We set  $N = 10d$  and evaluate different methods in terms of  $\text{MSE}_x$ ,

Table 3: The optimization performance of different methods in the three synthetic settings.

		Setting (1)			Setting (2)			Setting (3)		
		$MSE_x$	$MAE_y$	Acc	$MSE_x$	$MAE_y$	Acc	$MSE_x$	$MAE_y$	Acc
BO	TOBO	0.0000	0.0008	-	0.0003	0.0350	-	0.0001	0.0050	-
	sMTGP-UCB	0.0001	0.0031	-	0.0003	0.0361	-	0.0048	0.0590	-
	MLGP-UCB	0.0433	0.3793	-	0.0512	0.9295	-	0.0342	0.6263	-
	MVGP-UCB	0.0015	0.0523	-	0.0044	0.0550	-	0.0342	0.6263	-
	TOGP-RS	0.0893	0.3145	-	0.0026	0.0351	-	0.0106	0.1526	-
	sMTGP-RS	0.0251	0.3242	-	0.0206	0.3684	-	0.0084	0.1223	-
	MLGP-RS	0.0433	0.3793	-	0.0435	0.7976	-	0.0075	0.0934	-
	MVGP-RS	0.0148	0.2036	-	0.0157	0.2697	-	0.0084	0.1223	-
CBBO	TOCBBO	0.0023	0.0172	1.00	0.0000	0.0000	1.00	0.0021	0.0145	1.00
	sMTGP-UCB	0.1832	0.5614	0.67	0.0000	0.0000	1.00	0.0075	0.2171	0.86
	MLGP-UCB	0.0667	0.6527	0.33	0.1826	0.0779	1.00	0.2070	0.7105	0.43
	MVGP-UCB	0.0032	0.0285	1.00	0.0725	0.0312	1.00	0.0151	0.1988	0.71
	TOGP-RS	0.0438	0.5319	0.67	0.0908	0.0395	1.00	0.0512	0.8793	0.43
	sMTGP-RS	0.3151	0.5882	0.67	0.1826	0.0779	1.00	0.0117	0.9453	0.29
	MLGP-RS	0.1053	0.6909	0.33	0.1826	0.0779	1.00	0.0117	0.9453	0.29
	MVGP-RS	0.1313	0.5975	0.33	0.1489	0.0654	0.00	0.0512	0.8793	0.43

$MAE_y$ , and Acc, as defined in Appendix K. It is evident that for each GP, its UCB-based sampling strategy consistently outperforms its random sampling strategy. This is intuitive due to UCB’s better theoretical guarantees. Across all the GPs, our proposed TOBO and TOCBBO methods have the smallest  $MSE_x$  and  $MAE_y$ , indicating our selected super-arm and queried input points, together with the consequent output are closest to the true optimum. As to the other three GP-based methods, sMTGP-UCB achieves the second-best performance, followed by MVGP-UCB, while MLGP-UCB performs the worst. This result is consistent with their modeling abilities shown in Table 2.

Finally, we provide each round’s logarithmic instantaneous regret for different methods for BO and CBBO in Figure 1. We can observe that our TOBO and TOCBBO consistently

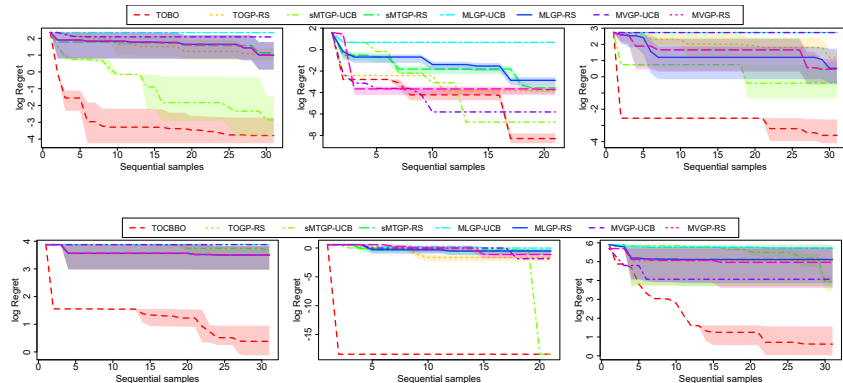


Figure 1: Each round’s logarithmic instantaneous regret of different methods in the Setting (1) (L), (2) (M), and (3) (R) for BO (Top row) and CBBO (Bottom row).

achieve the lowest instantaneous regret across all three settings, highlighting their superiority. Some additional results of synthetic experiments are presented in Appendix M.

## 5.2 Case studies

We further apply the proposed TOBO and TOBBO to four real-world datasets: (1) CHEM (Shields et al., 2021): input  $\mathbf{x} \in \mathbb{R}^2$  and output  $\mathbf{y} \in \mathbb{R}^{4 \times 3 \times 3}$ ; (2) MAT (Wang et al., 2020): input  $\mathbf{x} \in \mathbb{R}^4$  and output  $\mathbf{y} \in \mathbb{R}^{5 \times 4 \times 4}$ ; (3) PRINT (Zhai et al., 2023): input  $\mathbf{x} \in \mathbb{R}^5$  and output  $\mathbf{y} \in \mathbb{R}^{3 \times 4 \times 3}$ ; (4) REEN: input  $\mathbf{x} \in \mathbb{R}^6$  and output  $\mathbf{y} \in \mathbb{R}^{10 \times 2}$ . A detailed description of these datasets is provided in Appendix K. Since the renewable energy dataset provides fully observed data, we first evaluate the modeling performance of different GP surrogates

by training on 30 samples and testing on 5 samples randomly selected from the input space. The predictive performance of the four GP models on the testing data is reported in Table 4, and TOGP achieves the best predictive accuracy. As to the optimization performance of different methods for BO and CBBO, Figure 2 shows that our proposed TOBO and TOCBBO also consistently perform the best, demonstrating our applicability in complex real-world blackbox systems.

Table 4: The prediction performance of GPs in the REEN dataset.

	TOGP	sMTGP	MLGP	MVGP
NLL	15.6664	33.3198	88.2722	48.7167
MAE	0.0883	0.0993	0.0929	0.1054
$\ \text{Cov}\ $	0.4918	0.3555	0.4318	0.3711

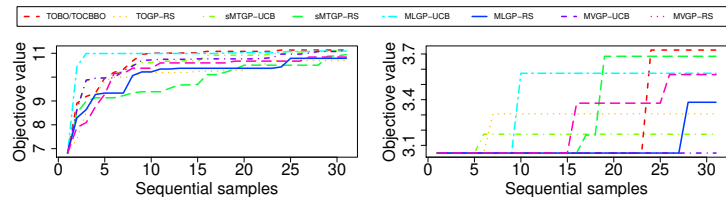


Figure 2: Each round’s optimal objective value in REEN for BO (L) and CBBO (R).

For the other three datasets, since they only contain partially observed data, we only evaluate their optimization performance under CBBO. Figure 2 shows that TOCBBO can identify the optimal input consistently using fewer rounds than the baselines, further demonstrating its superior effectiveness.

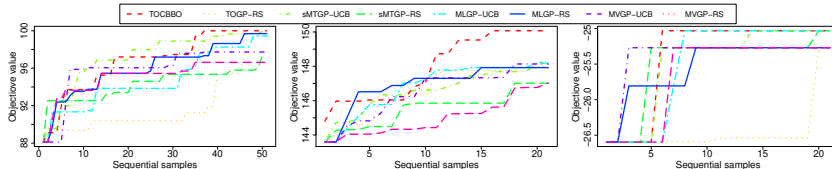


Figure 3: Each round’s optimal objective value in CHEM (L), MAT (M), and PRINT (R).

## 6 Conclusion and discussion

In this work, we propose two BO methods for tensor-output systems: TOBO employs two classes of kernel-based TOGP as a surrogate model and selects query points using a UCB acquisition function. TOCBBO extends TOGP to the partially observed setting and adopts a CMAB-UCB2 criterion to sequentially select both the query input and the super-arm. We establish theoretical regret bounds for both methods and demonstrate their effectiveness through extensive synthetic and real-world experiments. Future work could consider integrating the proposed tensor-output kernels with sparse techniques, such as sparse GPs (Snelson & Ghahramani, 2005) and scalable LMC (Bruinsma et al., 2020), to improve the computational efficiency of TOGP. The design of new acquisition functions can also be explored within this framework. For example, one may combine the TOGP model with EI or PI with theoretical guarantees (Frazier, 2018), and further extend them to the TOCBBO framework. In addition, improvement-based acquisition functions (Uhrenholt & Jensen, 2019) and information-theoretic criteria (Tu et al., 2022) may also be considered in our framework, provided that the computational challenges associated with tensor outputs can be effectively addressed. Finally, it is worth exploring more meaningful tensor structures for our proposed framework, such as a spatiotemporal system.

### Ethics statement

This work adheres to the ICLR Code of Ethics. Our study does not involve human subjects, sensitive personal information, or applications with immediate potential for harm. The

datasets used are publicly available or synthetically generated, and all experiments comply with community standards of fairness, transparency, and research integrity. We are not aware of any conflicts of interest, sponsorship issues, or ethical risks associated with this research. The use of large language models (LLMs) was restricted solely to polishing the writing, as described in Appendix A, and did not contribute to scientific content or results.

## Reproducibility statement

We have made extensive efforts to ensure reproducibility. All theoretical results are stated under explicit assumptions, with complete proofs provided in the appendix. Algorithmic procedures, including TOBO and TOCBO, are fully described in the main paper, with pseudocode and computational complexity analysis included in Appendix D. Experimental settings, dataset details, and evaluation metrics are reported in Section 5 and Appendix K. Synthetic datasets are specified in detail, and real-world datasets are publicly available with references provided. Source code and instructions for reproducing all experiments are included in the supplementary materials.

## References

Karim Abed-Meraiam, Nguyen Linh Trung, Adel Hafiane, et al. A contemporary and comprehensive survey on streaming tensor decomposition. *IEEE Transactions on Knowledge and Data Engineering*, 35(11):10897–10921, 2022.

Guglielmo Maria Accabi, Francesco Trovo, Alessandro Nuara, Nicola Gatti, and Marcello Restelli. When gaussian processes meet combinatorial bandits: Gcb. In 14th European Workshop on Reinforcement Learning, pp. 1–11, 2018.

Peter Auer, Nicolo Cesa-Bianchi, Yoav Freund, and Robert E Schapire. The nonstochastic multiarmed bandit problem. *SIAM journal on computing*, 32(1):48–77, 2002.

Syrine Belakaria, Aryan Deshwal, and Janardhan Rao Doppa. Max-value entropy search for multi-objective bayesian optimization. *Advances in neural information processing systems*, 32, 2019.

Mikhail Belyaev, Evgeny Burnaev, and Yermek Kapushev. Gaussian process regression for structured data sets. In *International Symposium on Statistical Learning and Data Sciences*, pp. 106–115. Springer, 2015.

Léon Bottou. Large-scale machine learning with stochastic gradient descent. *Proc. of COMPSTAT*, 01 2010.

Wessel Bruinsma, Eric Perim, William Tebbutt, Scott Hosking, Arno Solin, and Richard Turner. Scalable exact inference in multi-output gaussian processes. In *International Conference on Machine Learning*, pp. 1190–1201. PMLR, 2020.

Adam D Bull. Convergence rates of efficient global optimization algorithms. *Journal of Machine Learning Research*, 12(10), 2011.

Zexun Chen, Bo Wang, and Alexander N Gorban. Multivariate gaussian and student-t process regression for multi-output prediction. *Neural Computing and Applications*, 32: 3005–3028, 2020.

Eric C Chi and Tamara G Kolda. On tensors, sparsity, and nonnegative factorizations. *SIAM Journal on Matrix Analysis and Applications*, 33(4):1272–1299, 2012.

Sayak Ray Chowdhury and Aditya Gopalan. No-regret algorithms for multi-task bayesian optimization. In *International Conference on Artificial Intelligence and Statistics*, pp. 1873–1881. PMLR, 2021.

Tinkle Chugh. Scalarizing functions in bayesian multiobjective optimization. In *2020 IEEE Congress on Evolutionary Computation (CEC)*, pp. 1–8. IEEE, 2020.

Sihui Dai, Jialin Song, and Yisong Yue. Multi-task bayesian optimization via gaussian process upper confidence bound. In ICML 2020 workshop on real world experiment design and active learning, volume 60, pp. 61, 2020.

Samuel Daulton, Maximilian Balandat, and Eytan Bakshy. Differentiable expected hypervolume improvement for parallel multi-objective bayesian optimization. Advances in Neural Information Processing Systems, 33:9851–9864, 2020.

Samuel Daulton, David Eriksson, Maximilian Balandat, and Eytan Bakshy. Multi-objective bayesian optimization over high-dimensional search spaces. In Uncertainty in Artificial Intelligence, pp. 507–517. PMLR, 2022a.

Samuel Daulton, Xingchen Wan, David Eriksson, Maximilian Balandat, Michael A Osborne, and Eytan Bakshy. Bayesian optimization over discrete and mixed spaces via probabilistic reparameterization. Advances in Neural Information Processing Systems, 35:12760–12774, 2022b.

Vin De Silva and Lek-Heng Lim. Tensor rank and the ill-posedness of the best low-rank approximation problem. SIAM Journal on Matrix Analysis and Applications, 30(3):1084–1127, 2008.

Peter I Frazier. A tutorial on bayesian optimization. arXiv preprint arXiv:1807.02811, 2018.

Thomas E Fricker, Jeremy E Oakley, and Nathan M Urban. Multivariate gaussian process emulators with nonseparable covariance structures. Technometrics, 55(1):47–56, 2013.

José Henrique de M Goulart, Maxime Boizard, Rémy Boyer, Gérard Favier, and Pierre Comon. Tensor cp decomposition with structured factor matrices: Algorithms and performance. IEEE Journal of Selected Topics in Signal Processing, 10(4):757–769, 2015.

Daniel Hernández-Lobato, Jose Hernandez-Lobato, Amar Shah, and Ryan Adams. Predictive entropy search for multi-objective bayesian optimization. In International conference on machine learning, pp. 1492–1501. PMLR, 2016.

José Miguel Hernández-Lobato, Matthew W Hoffman, and Zoubin Ghahramani. Predictive entropy search for efficient global optimization of black-box functions. Advances in neural information processing systems, 27, 2014.

Dave Higdon. Space and space-time modeling using process convolutions. In Quantitative methods for current environmental issues, pp. 37–56. Springer, 2002.

Dionissios T Hristopulos. Non-separable covariance kernels for spatiotemporal gaussian processes based on a hybrid spectral method and the harmonic oscillator. IEEE Transactions on Information Theory, 70(2):1268–1283, 2023.

Congfang Huang, Jaesung Lee, Yang Zhang, Shiyu Zhou, and Jiong Tang. Mixed-input bayesian optimization method for structural damage diagnosis. IEEE Transactions on Reliability, 72(2):678–691, 2022.

Seyed Mostafa Kia, Christian F Beckmann, and Andre F Marquand. Scalable multi-task gaussian process tensor regression for normative modeling of structured variation in neuroimaging data. arXiv preprint arXiv:1808.00036, 2018.

Yongxiang Li and Qiang Zhou. Pairwise meta-modeling of multivariate output computer models using nonseparable covariance function. Technometrics, 58(4):483–494, 2016.

Eric F Lock. Tensor-on-tensor regression. Journal of Computational and Graphical Statistics, 27(3):638–647, 2018.

Wesley J Maddox, Maximilian Balandat, Andrew G Wilson, and Eytan Bakshy. Bayesian optimization with high-dimensional outputs. Advances in neural information processing systems, 34:19274–19287, 2021.

Dang Nguyen, Sunil Gupta, Santu Rana, Alistair Shilton, and Svetha Venkatesh. Bayesian optimization for categorical and category-specific continuous inputs. In Proceedings of the AAAI Conference on Artificial Intelligence, volume 34, pp. 5256–5263, 2020.

Ivan V Oseledets. Tensor-train decomposition. *SIAM Journal on Scientific Computing*, 33(5):2295–2317, 2011.

Omiros Papaspiliopoulos. High-dimensional probability: An introduction with applications in data science, 2020.

Binxin Ru, Ahsan Alvi, Vu Nguyen, Michael A Osborne, and Stephen Roberts. Bayesian optimisation over multiple continuous and categorical inputs. In International Conference on Machine Learning, pp. 8276–8285. PMLR, 2020.

Thomas J Santner, Brian J Williams, William I Notz, and Brian J Williams. The design and analysis of computer experiments, volume 1. Springer, 2003.

Pier Giuseppe Sessa, Pierre Laforgue, Nicolò Cesa-Bianchi, and Andreas Krause. Multitask learning with no regret: from improved confidence bounds to active learning. *Advances in Neural Information Processing Systems*, 36:6770–6781, 2023.

Benjamin J Shields, Jason Stevens, Jun Li, Marvin Parasram, Farhan Damani, Jesus I Martinez Alvarado, Jacob M Janey, Ryan P Adams, and Abigail G Doyle. Bayesian reaction optimization as a tool for chemical synthesis. *Nature*, 590(7844):89–96, 2021.

Edward Snelson and Zoubin Ghahramani. Sparse gaussian processes using pseudo-inputs. *Advances in neural information processing systems*, 18, 2005.

Jasper Snoek, Hugo Larochelle, and Ryan P Adams. Practical bayesian optimization of machine learning algorithms. *Advances in neural information processing systems*, 25, 2012.

Lei Song, Ke Xue, Xiaobin Huang, and Chao Qian. Monte carlo tree search based variable selection for high dimensional bayesian optimization. *Advances in Neural Information Processing Systems*, 35:28488–28501, 2022.

Qingquan Song, Hancheng Ge, James Caverlee, and Xia Hu. Tensor completion algorithms in big data analytics. *ACM Transactions on Knowledge Discovery from Data (TKDD)*, 13(1):1–48, 2019.

Niranjan Srinivas, Andreas Krause, Sham M Kakade, and Matthias Seeger. Gaussian process optimization in the bandit setting: No regret and experimental design. *arXiv preprint arXiv:0912.3995*, 2009.

Ben Tu, Axel Gandy, Nikolas Kantas, and Behrang Shafei. Joint entropy search for multi-objective bayesian optimization. *Advances in Neural Information Processing Systems*, 35:9922–9938, 2022.

Anders Kirk Uhrenholt and Bjøern Sand Jensen. Efficient bayesian optimization for target vector estimation. In The 22nd International Conference on Artificial Intelligence and Statistics, pp. 2661–2670. PMLR, 2019.

Boqian Wang, Jiacheng Cai, Chuangui Liu, Jian Yang, and Xianting Ding. Harnessing a novel machine-learning-assisted evolutionary algorithm to co-optimize three characteristics of an electrospun oil sorbent. *ACS Applied Materials & Interfaces*, 12(38):42842–42849, 2020.

Xilu Wang, Yaochu Jin, Sebastian Schmitt, and Markus Olhofer. Recent advances in bayesian optimization. *ACM Computing Surveys*, 55(13s):1–36, 2023.

Yan Wang, Meng Wang, Areej AlBahar, and Xiaowei Yue. Nested bayesian optimization for computer experiments. *IEEE/ASME Transactions on Mechatronics*, 28(1):440–449, 2022.

Christopher Williams and Matthias Seeger. Using the nyström method to speed up kernel machines. *Advances in neural information processing systems*, 13, 2000.

Jian Wu, Matthias Poloczek, Andrew G Wilson, and Peter Frazier. Bayesian optimization with gradients. *Advances in neural information processing systems*, 30, 2017.

Rose Yu, Guangyu Li, and Yan Liu. Tensor regression meets gaussian processes. In *International conference on artificial intelligence and statistics*, pp. 482–490. PMLR, 2018.

Cuihong Zhai, Jianjun Wang, Yiliu Paul Tu, Gang Chang, Xiaolei Ren, and Chunfeng Ding. Robust optimization of 3d printing process parameters considering process stability and production efficiency. *Additive Manufacturing*, 71:103588, 2023.

Yunchuan Zhang, Sangwoo Park, and Osvaldo Simeone. Multi-fidelity bayesian optimization with across-task transferable max-value entropy search. *IEEE Transactions on Signal Processing*, 2025.

Shandian Zhe, Wei Xing, and Robert M Kirby. Scalable high-order gaussian process regression. In *The 22nd International Conference on Artificial Intelligence and Statistics*, pp. 2611–2620. PMLR, 2019.

## A Use of LLMs

Large Language Models (LLMs) were used to aid in the writing and polishing of the manuscript. Specifically, we used an LLM to assist in refining the language, improving readability, and ensuring clarity in various sections of the paper. The model helped with tasks such as sentence rephrasing, grammar checking, and enhancing the overall flow of the text.

It is important to note that the LLM was not involved in the ideation, research methodology, or experimental design. All research concepts, ideas, and analyses were developed and conducted by the authors. The contributions of the LLM were solely focused on improving the linguistic quality of the paper, with no involvement in the scientific content or data analysis.

The authors take full responsibility for the content of the manuscript, including any text generated or polished by the LLM. We have ensured that the LLM-generated text adheres to ethical guidelines and does not contribute to plagiarism or scientific misconduct.

## B The details of the tensor decomposition in Remark 1

As discussed in Remark 1, directly estimating the entries of the core tensors  $\{\mathbf{A}_l\}_{l=1}^m$  or  $\mathbf{A}$  requires  $mT$  parameters for the non-separable tensor-output kernel and  $T$  parameters for the separable tensor-output kernel, which becomes intractable for large-scale or high-order tensors. To reduce this complexity, we impose low-rank tensor structures. In particular, we adopt different decompositions depending on the tensor order.

Low-order tensors ( $m \leq 3$ ): When the tensor order is small, we employ the CP decomposition:

$$\mathbf{A}_l = \sum_{r=1}^{R_l} \mathbf{a}_{lr1} \circ \mathbf{a}_{lr2} \circ \cdots \circ \mathbf{a}_{lrm} \quad \text{for non-separable tensor-output kernel,} \quad (17)$$

$$\mathbf{A} = \sum_{r=1}^R \mathbf{a}_{r1} \circ \mathbf{a}_{r2} \circ \cdots \circ \mathbf{a}_{rm} \quad \text{for separable tensor-output kernel,} \quad (18)$$

where  $\mathbf{a}_{lri}, \mathbf{a}_{ri} \in \mathbb{R}^{t_i}$  for  $r = 1, \dots, R$  and  $i = 1, \dots, m$  for  $r = 1, \dots, R$  and  $i = 1, \dots, m$ . The number of free parameters is  $\sum_{l=1}^m \sum_{i=1}^m R_l t_i$  for the non-separable tensor-output kernel in (6) and  $R \sum_{i=1}^m t_i$  for the separable tensor-output kernel in (7), which grows only linearly in

each mode size  $t_i$ . Thus, CP provides a very compact representation when  $m \leq 3$ . However, CP decomposition is often ill-posed for higher-order tensors, since the set of tensors of fixed CP rank is not closed, implying that a best low-rank approximation may not exist (De Silva & Lim, 2008). In addition, the factor matrices can easily become ill-conditioned as  $m$  increases, leading to numerical instability (Chi & Kolda, 2012).

High-order tensors ( $m > 3$ ): When the tensor order is large, we employ the TT decomposition:

$$\mathbf{A}_l = \mathbf{G}_{l1}(t_1)\mathbf{G}_{l2}(t_2) \cdots \mathbf{G}_{lm}(t_m) \quad \text{for non-separable tensor-output kernel,} \quad (19)$$

$$\mathbf{A} = \mathbf{G}_1(t_1)\mathbf{G}_2(t_2) \cdots \mathbf{G}_m(t_m) \quad \text{for separable tensor-output kernel,} \quad (20)$$

where each  $\mathbf{G}_{lj}(t_j)$  is a  $r_{l,j-1} \times t_j \times r_{l,j}$  three-mode tensor and the TT-ranks satisfy  $r_{l,0} = r_{l,m} = 1$  for  $l = 1, \dots, m$ . Similarly,  $\mathbf{G}_j(t_j)$  is a  $r_{j-1} \times t_j \times r_j$  three-mode tensor that satisfies  $r_0 = r_m = 1$ . The total number of free parameters is  $\sum_{l=1}^m \sum_{j=1}^m r_{l,j-1} t_j r_{l,j}$  for the non-separable tensor-output kernel in (6) and  $\sum_{j=1}^m r_{j-1} t_j r_j$  for the separable tensor-output kernel in (7). It scales linearly with the tensor order  $m$ , instead of exponentially as in the full tensor. This makes TT decomposition highly suitable for high-order tensors ( $m > 3$ ), as it balances modeling flexibility with computational scalability and avoids the instability of CP.

Therefore, in our framework, we adopt CP decomposition-based for low-order cores and TT decomposition-based for high-order cores, ensuring both efficiency and robustness across different tensor settings.

## C The estimation of hyperparameters for the TOGP and PTOGP

In this appendix, we provide the details of hyperparameter estimation for both TOGP and PTOGP. Without loss of generality, we assume a zero prior mean  $\boldsymbol{\mu} = 0$  in (3) and (12).

### C.1 Parameter estimation for training TOGP

Given the training data  $\mathbf{X}_n = (\mathbf{x}_1, \dots, \mathbf{x}_n)$  and  $\mathbf{Y}_n = (vec(\mathbf{y}_1)^\top, \dots, vec(\mathbf{y}_n)^\top)^\top$ , the log marginal likelihood of TOGP is given by:

$$\log L(\boldsymbol{\Theta}) = -\frac{1}{2} \log |\boldsymbol{\Sigma}_n| - \frac{1}{2} \mathbf{Y}_n^\top \boldsymbol{\Sigma}_n^{-1} \mathbf{Y}_n, \quad (21)$$

where  $\boldsymbol{\Sigma}_n = \sigma^2 \mathbf{K}_n + \tau^2 \mathbf{I}_{nT}$ . Then, (21) can be optimized by applying gradient-based optimization methods, such as L-BFGS algorithm.

The gradients of the log-likelihood function in (21) with respect to the hyperparameters  $\tau^2$ ,  $\sigma^2$ ,  $\boldsymbol{\theta}$ , and  $\mathbf{a}$  is given by

$$\frac{\partial \log L}{\partial \tau^2} = \frac{1}{2} \text{tr}(\boldsymbol{\Sigma}_n^{-1} \mathbf{K}_n) - \frac{1}{2} \mathbf{Y}_n^\top \boldsymbol{\Sigma}_n^{-1} \mathbf{K}_n \boldsymbol{\Sigma}_n^{-1} \mathbf{Y}_n, \quad (22)$$

$$\frac{\partial \log L}{\partial \sigma^2} = \frac{1}{2} \text{tr}(\boldsymbol{\Sigma}_n^{-1}) - \frac{1}{2} \mathbf{Y}_n^\top \boldsymbol{\Sigma}_n^{-1} \boldsymbol{\Sigma}_n^{-1} \mathbf{Y}_n, \quad (23)$$

$$\frac{\partial \log L}{\partial \theta_{lij}} = \frac{\tau^2}{2} \text{tr}\left(\boldsymbol{\Sigma}_n^{-1} \frac{\partial \mathbf{K}_n}{\partial \theta_{lij}}\right) - \frac{\tau^2}{2} \mathbf{Y}_n^\top \boldsymbol{\Sigma}_n^{-1} \frac{\partial \mathbf{K}_n}{\partial \theta_{lij}} \boldsymbol{\Sigma}_n^{-1} \mathbf{Y}_n, \quad (24)$$

$$\frac{\partial \log L}{\partial a_{lij}} = \frac{1}{2} \text{tr}\left(\boldsymbol{\Sigma}_n^{-1} \tau^2 \frac{\partial \mathbf{K}_n}{\partial a_{lij}}\right) - \frac{\tau^2}{2} \mathbf{Y}_n^\top \boldsymbol{\Sigma}_n^{-1} \frac{\partial \mathbf{K}_n}{\partial a_{lij}} \boldsymbol{\Sigma}_n^{-1} \mathbf{Y}_n, \quad (25)$$

where  $\theta_{lij}$  represents the scale parameters of  $k_{lj}$ , the kernel function associated with the  $l$ -th mode. The matrices  $\frac{\partial \mathbf{K}_n}{\partial \theta_{lij}}$  and  $\frac{\partial \mathbf{K}_n}{\partial a_{lij}}$  are the partial derivatives of the kernel matrix with respect to the corresponding kernel parameters.

The detailed algorithm for training TOGP is given as follows:

## Algorithm 1 Parameter estimation for training TOGP

---

Input: Training data  $\mathbf{X}_n$  and  $\mathbf{Y}_n$ , initial hyperparameters  $\Theta_0 = \{\sigma_0^2, \tau_0^2, \boldsymbol{\theta}_0, \mathbf{a}_0\}$ ;  
 Initialize:  $\sigma^2 \leftarrow \sigma_0^2, \tau^2 \leftarrow \tau_0^2, \boldsymbol{\theta} \leftarrow \boldsymbol{\theta}_0, \mathbf{a} \leftarrow \mathbf{a}_0$ ;  
 1: while  $\tau^2, \sigma^2, \boldsymbol{\theta}, \mathbf{a}$  not converge do  
 2:   Update  $\tau^2$  based on (22);  
 3:   Update  $\sigma^2$  based on (23);  
 4:   Update  $\boldsymbol{\theta}$  based on (24);  
 5:   Update  $\mathbf{a}$  based on (25).  
 6: end while

---

Remark 4. For the non-separable tensor-output kernel in Definition 1, the total number of hyperparameters to be estimated in TOGP is  $m_h = 2 + T + \sum_{l=1}^m \sum_{i=1}^m R_l t_i$  when  $m \leq 3$  and  $m_h = 2 + T + \sum_{l=1}^m \sum_{j=1}^m r_{l,j-1} t_j r_{l,j}$  when  $m > 3$ . For the separable tensor-output kernel in Definition 2, the total number of hyperparameters to be estimated in TOGP is  $m_h = 2 + T + R \sum_{i=1}^m t_i$  when  $m \leq 3$  and  $m_h = 2 + T + \sum_{j=1}^m r_{j-1} t_j r_j$  when  $m > 3$ . The computational complexity of computing the gradient of  $\log L(\Theta)$  with respect to all  $m_h$  parameters is  $\mathcal{O}(n^3 T^3 + n^2 T^2 m_h)$ . When using the L-BFGS algorithm to optimize the likelihood function results, the number of iterations typically scales as  $\mathcal{O}(\log(n))$  (Bottou, 2010). Therefore, the overall computational complexity for training the TOGP takes  $\mathcal{O}(n^3 T^3 \log(n) + n^2 T^2 m_h \log(n))$  computational complexity.

## C.2 Parameter estimation for training PTOGP

Given the partially observed training data  $\mathbf{X}_n = (\mathbf{x}_1, \dots, \mathbf{x}_n)$ ,  $\boldsymbol{\Lambda}_n = (\boldsymbol{\lambda}_1, \dots, \boldsymbol{\lambda}_n)^\top$ , and  $\tilde{\mathbf{Y}}_n = (\tilde{\mathbf{y}}_1, \dots, \tilde{\mathbf{y}}_n)^\top$ , the log marginal likelihood of PTOGP is given by:

$$\log \tilde{L}(\Theta) = -\frac{1}{2} \log |\tilde{\boldsymbol{\Sigma}}_n| - \frac{1}{2} \text{vec}(\tilde{\mathbf{Y}}_n)^\top \tilde{\boldsymbol{\Sigma}}_n^{-1} \text{vec}(\tilde{\mathbf{Y}}_n), \quad (26)$$

where  $\tilde{\boldsymbol{\Sigma}}_n = \sigma^2 \mathbf{E}_n \mathbf{K}_n \mathbf{E}_n^\top + \tau^2 \mathbf{I}_{nk}$ . Then, (26) can also be optimized by applying gradient-based optimization methods.

The gradients of the log-likelihood function in (26) with respect to the hyperparameters  $\sigma^2$ ,  $\tau^2$ ,  $\boldsymbol{\theta}$ , and  $\mathbf{a}$  is given by

$$\frac{\partial \tilde{L}}{\partial \tau^2} = \frac{1}{2} \text{tr} \left( \tilde{\boldsymbol{\Sigma}}_n^{-1} \mathbf{E}_n \mathbf{K}_n \mathbf{E}_n^\top \right) - \frac{1}{2} \tilde{\mathbf{Y}}_n^\top \tilde{\boldsymbol{\Sigma}}_n^{-1} \mathbf{E}_n \mathbf{K}_n \mathbf{E}_n^\top \tilde{\boldsymbol{\Sigma}}_n^{-1} \tilde{\mathbf{Y}}_n, \quad (27)$$

$$\frac{\partial \tilde{L}}{\partial \sigma^2} = \frac{1}{2} \text{tr} \left( \tilde{\boldsymbol{\Sigma}}_n^{-1} \right) - \frac{1}{2} \tilde{\mathbf{Y}}_n^\top \tilde{\boldsymbol{\Sigma}}_n^{-1} \tilde{\boldsymbol{\Sigma}}_n^{-1} \tilde{\mathbf{Y}}_n, \quad (28)$$

$$\frac{\partial \tilde{L}}{\partial \theta_{lij}} = \frac{\tau^2}{2} \text{tr} \left( \tilde{\boldsymbol{\Sigma}}_n^{-1} \mathbf{E}_n \frac{\partial \mathbf{K}_n}{\partial \theta_{lij}} \mathbf{E}_n^\top \right) - \frac{\tau^2}{2} \tilde{\mathbf{Y}}_n^\top \tilde{\boldsymbol{\Sigma}}_n^{-1} \mathbf{E}_n \frac{\partial \mathbf{K}_n}{\partial \theta_{lij}} \mathbf{E}_n^\top \tilde{\boldsymbol{\Sigma}}_n^{-1} \tilde{\mathbf{Y}}_n, \quad (29)$$

$$\frac{\partial \tilde{L}}{\partial a_{lij}} = \frac{\tau^2}{2} \text{tr} \left( \tilde{\boldsymbol{\Sigma}}_n^{-1} \mathbf{E}_n \frac{\partial \mathbf{K}_n}{\partial a_{lij}} \mathbf{E}_n^\top \right) - \frac{\tau^2}{2} \tilde{\mathbf{Y}}_n^\top \tilde{\boldsymbol{\Sigma}}_n^{-1} \mathbf{E}_n \frac{\partial \mathbf{K}_n}{\partial a_{lij}} \mathbf{E}_n^\top \tilde{\boldsymbol{\Sigma}}_n^{-1} \tilde{\mathbf{Y}}_n, \quad (30)$$

The detailed algorithm for training PTOGP is given as follows:

## Algorithm 2 Parameter estimation for training PTOGP

---

Input: Training data  $\mathbf{X}_n$ ,  $\boldsymbol{\Lambda}_n$  and  $\tilde{\mathbf{Y}}_n$ , initial hyperparameters  $\Theta_0 = \{\sigma_0^2, \tau_0^2, \boldsymbol{\theta}_0, \mathbf{a}_0\}$ ;  
 Initialize:  $\sigma^2 \leftarrow \sigma_0^2, \tau^2 \leftarrow \tau_0^2, \boldsymbol{\theta} \leftarrow \boldsymbol{\theta}_0, \mathbf{a} \leftarrow \mathbf{a}_0$ ;  
 1: while  $\sigma^2, \tau^2, \boldsymbol{\theta}, \mathbf{a}$  not converge do  
 2:   Update  $\tau^2$  based on (27);  
 3:   Update  $\sigma^2$  based on (28);  
 4:   Update  $\boldsymbol{\theta}$  based on (29);  
 5:   Update  $\mathbf{a}$  based on (30).  
 6: end while

---

Remark 5. For the non-separable tensor-output kernel in Definition 1, the total number of hyperparameters to be estimated in PTOGP is  $m_h = 2 + T + \sum_{l=1}^m \sum_{i=1}^m R_l t_i$  when  $m \leq 3$  and  $m_h = 2 + T + \sum_{l=1}^m \sum_{j=1}^m r_{l,j-1} t_j r_{l,j}$  when  $m > 3$ . For the separable tensor-output kernel in Definition 2, the total number of hyperparameters to be estimated in PTOGP is  $m_h = 2 + T + R \sum_{i=1}^m t_i$  when  $m \leq 3$  and  $m_h = 2 + T + \sum_{j=1}^m r_{j-1} t_j r_j$  when  $m > 3$ .

The computational complexity of computing the gradient of  $\tilde{L}(\Theta)$  with respect to all  $m_h$  parameters is  $\mathcal{O}(k^3 T^3 + n^2 k T m_h)$ . When using the L-BFGS algorithm to optimize the likelihood function results, the number of iterations typically scales as  $\mathcal{O}(\log(n))$  Bottou (2010). Therefore, the overall computational complexity for training the PTOGP takes  $\mathcal{O}(n^3 k^3 \log(n) + n^2 k T m_h \log(n))$  computational complexity.

## D The proposed algorithms and computational complexity analysis

### D.1 UCB-based TOBO algorithm

The detailed procedure of the proposed TOBO method is given in Algorithm 3.

---

#### Algorithm 3 UCB-based TOBO

---

Input: Total rounds  $N$ , initial dataset  $\mathcal{D}_0 = \emptyset$ , initial hyperparameters  $\Theta_0$ ;

- 1: for round  $n = 1, \dots, N$  do
- 2:   Update the posterior mean (4) and covariance (5) of  $\mathbf{f}$  given  $\Theta_{n-1}$ ;
- 3:   Select the next input  $\mathbf{x}_n \leftarrow \arg \max_{\mathbf{x} \in \mathcal{X}} \alpha_{UCB}(\mathbf{x} \mid \mathcal{D}_{n-1})$ ;
- 4:   Evaluate the black-box system and observe output  $\mathbf{y}_n$ ;
- 5:   Update dataset  $\mathcal{D}_n \leftarrow \mathcal{D}_{n-1} \cup \{\mathbf{x}_n, \mathbf{y}_n\}$ ;
- 6:   Update hyperparameters  $\Theta_n$  by maximizing (21) with L-BFGS;
- 7: end for
- 8: Identify  $i^* = \arg \max_{i \in [N]} L_f(\mathbf{x}_i)$ ;
- 9: Output: Optimal input  $\mathbf{x}_{i^*}$  and corresponding output  $\mathbf{y}_{i^*}$ .

---

Remark 6. When using the TOBO method to select  $\mathbf{x}^*$ , the computational complexity of updating TOGP is  $\mathcal{O}((n-1)^3 T^3)$  at round  $n$ . Then, the computational complexity of querying the next point is  $\mathcal{O}((n-1)^2 T^2 \log(n))$  by using the L-BFGS method. After updating the design dataset, the computational complexity of updating the hyperparameters  $\Theta$  is  $\mathcal{O}(n^3 T^3 \log(n) + n^2 T^2 m_h \log(n))$ . Thus, the computational complexity of TOBO at round  $n$  is  $\mathcal{O}(n^3 T^3 \log(n) + n^2 T^2 m_h \log(n))$ . Suppose that there are  $N$  points needed to query, the total computational complexity of Algorithm 3 is  $\mathcal{O}\left(\sum_{n=1}^N [n^3 T^3 \log(n) + n^2 T^2 m_h \log(n)]\right)$ .

### D.2 CMAB-UCB2-based TOCBBO algorithm

The detailed algorithm of TOCBBO is provided in Algorithm 4.

## Algorithm 4 CMAB-UCB2-based TOCBBO

---

Input: Total rounds  $N$ , initial dataset  $\tilde{\mathcal{D}}_0 = \emptyset$ , initial hyperparameters  $\Theta_0$ ;

- 1: for round  $n = 1, \dots, N$  do
- 2:   Update the posterior mean (13) and covariance (14);
- 3:   Select the next input  $\mathbf{x}_n$  using (15);
- 4:   Select the super-arm  $\boldsymbol{\lambda}_n$  using (16);
- 5:   Evaluate  $\mathbf{f}$  under  $(\mathbf{x}_n, \boldsymbol{\lambda}_n)$  and observe  $\tilde{\mathbf{y}}_n$ ;
- 6:   Update dataset  $\tilde{\mathcal{D}}_n \leftarrow \tilde{\mathcal{D}}_{n-1} \cup \{(\mathbf{x}_n, \boldsymbol{\lambda}_n), \tilde{\mathbf{y}}_n\}$ ;
- 7:   Update hyperparameters  $\Theta_n$  by maximizing  $\log \tilde{L}(\Theta)$  with L-BFGS;
- 8:   Update incumbent solution  $\{\mathbf{x}_n^*, \boldsymbol{\lambda}_n^*\} = \arg \max_{i=1, \dots, n} H_f \tilde{\mathbf{f}}(\mathbf{x}_i, \boldsymbol{\lambda}_i)$ ;
- 9: end for
- 10: Identify  $i^* = \arg \max_{i \in [N]} H_f \tilde{\mathbf{f}}(\mathbf{x}_i, \boldsymbol{\lambda}_i)$ ;
- 11: Output: Optimal input  $\mathbf{x}_{i^*}$ , optimal super-arm  $\boldsymbol{\lambda}_{i^*}$ , and output  $\tilde{\mathbf{y}}_{i^*}$ .

---

Remark 7. When using the proposed TOCBBO method to jointly select  $\mathbf{x}^*$  and  $\boldsymbol{\lambda}^*$ , the computational complexity of updating the PTOGP at round  $n$  is  $\mathcal{O}((n-1)^3 k^3)$ . Then, based on the proposed CMAB-UCB2 criterion, the computational complexity of querying the next input by using L-BFGS method is  $\mathcal{O}((n-1)^2 k^2)$  and selecting the next super-arm by using greedy Top- $k$  method is  $\mathcal{O}(kT^3)$ , respectively. After updating the current design dataset, the computational complexity of updating hyperparameters  $\Theta$  is  $\mathcal{O}(n^3 k^3 \log(n) + n^2 k T m_h \log(n))$ . Therefore, at round  $n$ , the computational complexity of TOCBBO method is  $\mathcal{O}(n^3 k^3 \log(n) + n^2 k T m_h \log(n) + kT^3)$ . Assuming a total of  $N$  rounds, the overall computational complexity of Algorithm 4 is  $\mathcal{O}\left(\sum_{n=1}^N [n^3 k^3 \log(n) + n^2 k T m_h \log(n) + kT^3]\right)$ .

## E The proof of Proposition 1

Proof. We prove symmetry and positive semi-definite for the two kernel classes in Definitions 1–2.

Non-separable kernel (Definition 1): Denote  $\mathbf{a}_\ell := \text{vec}(\mathbf{A}_\ell) \in \mathbb{R}^T$  (resp.  $\mathbf{a} := \text{vec}(\mathbf{A}) \in \mathbb{R}^T$ ). The tensor-output kernel is

$$\mathbf{K}(\mathbf{x}, \mathbf{x}') = \sum_{\ell=1}^m \sum_{j=1}^{t_\ell} \mathbf{a}_\ell \mathbf{a}_\ell^\top k_{\ell j}(\mathbf{x}, \mathbf{x}'), \quad \mathbf{x}, \mathbf{x}' \in \mathcal{X}, \quad (31)$$

where each  $k_{\ell j}$  is a scalar positive semi-definite kernel.

For any  $\mathbf{x}, \mathbf{x}' \in \mathcal{X}$ , we have

$$\begin{aligned} \mathbf{K}(\mathbf{x}, \mathbf{x}')^\top &= \sum_{\ell, j} (\mathbf{a}_\ell \mathbf{a}_\ell^\top)^\top k_{\ell j}(\mathbf{x}, \mathbf{x}') \\ &= \sum_{\ell, j} \mathbf{a}_\ell \mathbf{a}_\ell^\top k_{\ell j}(\mathbf{x}, \mathbf{x}') \\ &= \sum_{\ell, j} \mathbf{a}_\ell \mathbf{a}_\ell^\top k_{\ell j}(\mathbf{x}', \mathbf{x}) \\ &= \mathbf{K}(\mathbf{x}', \mathbf{x}), \end{aligned} \quad (32)$$

This shows that the full tensor-output kernel  $\mathbf{K}$  is symmetric.

Let  $\{\mathbf{x}_i\}_{i=1}^n \subset \mathcal{X}$  and  $\{\mathbf{y}_i\}_{i=1}^n \subset \mathbb{R}^T$  be arbitrary. Then, we have

$$\begin{aligned} \sum_{i, j=1}^n \mathbf{y}_i^\top \mathbf{K}(\mathbf{x}_i, \mathbf{x}_j) \mathbf{y}_j &= \sum_{\ell, j} \sum_{i, j} \mathbf{y}_i^\top (\mathbf{a}_\ell \mathbf{a}_\ell^\top) \mathbf{y}_j k_{\ell j}(\mathbf{x}_i, \mathbf{x}_j) \\ &= \sum_{\ell, j} \sum_{i, j} s_{\ell j, i} k_{\ell j}(\mathbf{x}_i, \mathbf{x}_j) s_{\ell j, j}, \end{aligned} \quad (33)$$

where  $s_{\ell j, i} := \mathbf{a}_\ell^\top \mathbf{y}_i \in \mathbb{R}$ . For each fixed  $(\ell, j)$ , the matrix  $[k_{\ell j}(\mathbf{x}_i, \mathbf{x}_j)]_{i,j=1}^n$  is positive semi-definite, so  $\sum_{i,j} s_{\ell j, i} k_{\ell j}(\mathbf{x}_i, \mathbf{x}_j) s_{\ell j, j} \geq 0$ . Summing over  $(\ell, j)$  preserves nonnegativity, hence the Gram matrix induced by  $\mathbf{K}$  is positive semi-definite.

Separable kernel (Definition 2): The kernel is

$$\mathbf{K}(\mathbf{x}, \mathbf{x}') = \mathbf{a} \mathbf{a}^\top k(\mathbf{x}, \mathbf{x}'), \quad \mathbf{x}, \mathbf{x}' \in \mathcal{X}, \quad (34)$$

where  $k$  is a scalar positive semi-definite kernel. Since  $(\mathbf{a} \mathbf{a}^\top)^\top = \mathbf{a} \mathbf{a}^\top$  and  $k(\mathbf{x}, \mathbf{x}') = k(\mathbf{x}', \mathbf{x})$ , we have  $\mathbf{K}(\mathbf{x}, \mathbf{x}')^\top = \mathbf{K}(\mathbf{x}', \mathbf{x})$ . For arbitrary  $\{\mathbf{x}_i\}_{i=1}^n$  and  $\{\mathbf{y}_i\}_{i=1}^n$ ,  $\sum_{i,j=1}^n \mathbf{y}_i^\top \mathbf{K}(\mathbf{x}_i, \mathbf{x}_j) \mathbf{y}_j = \sum_{i,j} (\mathbf{a}^\top \mathbf{y}_i) k(\mathbf{x}_i, \mathbf{x}_j) (\mathbf{a}^\top \mathbf{y}_j) \geq 0$ , because the Gram matrix  $[k(\mathbf{x}_i, \mathbf{x}_j)]$  is positive semi-definite.

Therefore, both kernel classes are symmetric and generate positive semi-definite Gram matrices for any finite set of inputs, i.e., they are valid tensor-output kernels on  $\mathcal{X}$ .  $\square$

## F The proof of Lemma 1

Proof. First, for a tensor-output system  $\text{vec}(\mathbf{f}(\mathbf{x}))$  following a TOGP defined in (3), denote the derivative field of  $\text{vec}(\mathbf{f}(\mathbf{x}))$  to the  $j$ -coordinate element of  $\mathbf{x}$  as  $\mathbf{g}_j(\mathbf{x}) := \partial \text{vec}(\mathbf{f}(\mathbf{x})) / \partial x_j$ , where  $\text{vec}(\mathbf{f}(\mathbf{x})) \in \mathbb{R}^T$  and  $j \in \{1, \dots, d\}$ . According to the derivative property of GP (Santner et al., 2003), we have that  $\mathbf{g}_j(\mathbf{x}) \in \mathbb{R}^T$  is a multivariate-output GP with mean  $\hat{\mu}_n^\nabla(x_j) := \frac{\partial}{\partial x_j} \mu_n(\mathbf{x})$  and covariance  $\hat{\mathbf{K}}_n^\nabla(x_j, x'_j) := \text{Cov}(\mathbf{g}_j(\mathbf{x}), \mathbf{g}_j(\mathbf{x}')) = \frac{\partial^2}{\partial x_j \partial x'_j} \sigma^2 \mathbf{K}(\mathbf{x}, \mathbf{x}')$ .

At round  $n + 1$ , the observed data is denoted as  $\mathbf{X}_n$  and  $\mathbf{Y}_n$ , then we have the posterior distribution of  $\mathbf{g}_j(\mathbf{x})$  is a  $T$ -dimensional Gaussian with mean and covariance

$$\hat{\mathbf{K}}_n^\nabla(x_j, x'_j) = \frac{\partial \hat{\mu}_n(\mathbf{x})}{\partial x_j} \quad (35)$$

$$\hat{\mathbf{K}}_n^\nabla(x_j, x'_j) = \frac{\partial^2 \hat{\mathbf{K}}_n(\mathbf{x}, \mathbf{x}')}{\partial x_j \partial x'_j}. \quad (36)$$

It is easy to verify that  $\hat{\mathbf{K}}_n^\nabla(x_j, x'_j)$  is positive semi-definite for every  $\mathbf{x}$ .

For any fixed  $\mathbf{x} \in \mathcal{X}$ , given  $\mathbf{X}_n$  and  $\mathbf{Y}_n$ , the random vector

$$\mathbf{g}_j(\mathbf{x}) - \hat{\mu}_n^\nabla(x_j) \sim \mathcal{N}(\mathbf{0}, \hat{\mathbf{K}}_n^\nabla(\mathbf{x}, \mathbf{x}; j)). \quad (37)$$

Applying the Gaussian Lipschitz concentration (Proposition 2.5.2 and Theorem 5.2.2 in Papaspiliopoulos (2020)) to the norm  $\|\cdot\|_2$  yields, for all  $t > 0$ ,

$$\Pr\left(\|\mathbf{g}_j(\mathbf{x}) - \hat{\mu}_n^\nabla(x_j)\| \geq \sqrt{\text{tr}(\hat{\mathbf{K}}_n^\nabla(x_j, x_j))} + t\right) \leq \exp\left(-\frac{t^2}{2 \lambda_{\max}^{(n)}(x_j)}\right), \quad (38)$$

where  $\lambda_{\max}^{(n)}(\mathbf{x}; j)$  is the largest eigenvalue of  $\hat{\mathbf{K}}_n^\nabla(\mathbf{x}, \mathbf{x}; j)$ .

Let  $\mathcal{D}_M = \{\mathbf{x}_1, \dots, \mathbf{x}_M\} \subset \mathcal{X}$  be any finite discretization. Using (38) with  $t(\mathbf{x}) = \sqrt{2 \lambda_{\max}^{(n)}(x_j) \log(M/\delta)}$ , and applying the union bound, we obtain with probability at least  $1 - \delta$ ,

$$\|\mathbf{g}_j(\mathbf{x}) - \hat{\mu}_n^\nabla(x_j)\| \leq \sqrt{\text{tr}(\hat{\mathbf{K}}_n^\nabla(x_j, x_j))} + \sqrt{2 \lambda_{\max}^{(n)}(x_j) \log(M/\delta)}, \quad \forall \mathbf{x} \in \mathcal{D}_M. \quad (39)$$

Let  $C_\nabla := \sup_{\mathbf{x} \in \mathcal{X}} \sqrt{\text{tr}(\hat{\mathbf{K}}_n^\nabla(x_j, x_j))}$  and  $\Lambda_\nabla := \sup_{\mathbf{x} \in \mathcal{X}} \lambda_{\max}^{(n)}(x_j)$ , then (39) implies that, with probability at least  $1 - \delta$ ,

$$\|\mathbf{g}_j(\mathbf{x})\| \leq \|\hat{\mu}_n^\nabla(x_j)\| + C_\nabla + \sqrt{2 \Lambda_\nabla \log(M/\delta)}, \quad \forall \mathbf{x} \in \mathcal{D}_M. \quad (40)$$

Assume the kernel is sufficiently smooth so that  $\mathbf{g}_j(\cdot)$  has almost surely Lipschitz sample paths. Then there exist absolute constants  $a, b > 0$  (depending on the Lipschitz modulus and a covering-number bound of  $\mathcal{X}$ ) such that for any  $L' > 0$ ,

$$\Pr\left(\sup_{\mathbf{x} \in \mathcal{X}} \|\mathbf{g}_j(\mathbf{x})\| > L' + C_\nabla\right) \leq a \exp\left(-\frac{(L')^2}{b^2}\right). \quad (41)$$

This follows by combining the net bound (40) with a standard chaining argument to pass from a finite net to the full domain; the Gaussian tail is preserved with a possible adjustment of absolute constants into  $a, b$ .  $\square$

## G The proof of Theorem 1

Proof. The proof consists of two main parts. We first establish a concentration inequality for  $\text{vec}(\mathbf{f}(\mathbf{x}))$  for any  $\mathbf{x} \in \mathcal{X}$ , and then use this result to derive an upper bound for the regret.

Part 1. Concentration inequality. We begin by proving a concentration inequality for  $\text{vec}(\mathbf{f}(\mathbf{x}))$  evaluation on a discrete set of points in the domain  $\mathcal{X}$ . We then extend the result to neighborhoods of these discrete points, and ultimately to the entire space  $\mathcal{X}$ .

We first prove a basic concentration inequality for a general  $T$ -dimensional Gaussian distribution, i.e.,  $\mathbf{Z} \sim \mathcal{N}(\boldsymbol{\mu}, \mathbf{K})$ . If we define  $\mathbf{U} = \mathbf{Z} - \boldsymbol{\mu}$  and set another  $T$ -dimensional standard Gaussian distribution  $\mathbf{V} \sim \mathcal{N}(0, \mathbf{I}_T)$ , we can obtain

$$\mathbf{U} \stackrel{d}{=} \mathbf{K}^{1/2}\mathbf{V}, \quad \|\mathbf{U}\| = \|\mathbf{K}^{1/2}\mathbf{V}\|.$$

Define the function  $f(\mathbf{U}) \triangleq \|\mathbf{K}^{1/2}\mathbf{V}\|$ . For any  $\mathbf{U}, \mathbf{U}'$ , we have

$$|f(\mathbf{U}) - f(\mathbf{U}')| \leq \|\mathbf{K}^{1/2}(\mathbf{U} - \mathbf{U}')\| \leq \|\mathbf{K}^{1/2}\|_{op} \|\mathbf{U} - \mathbf{U}'\| = \sqrt{\lambda_{\max}(\mathbf{K})} \|\mathbf{U} - \mathbf{U}'\|,$$

where  $\lambda_{\max}(\mathbf{K})$  is the maximum eigenvalue of  $\mathbf{K}$ . Therefore  $f$  is a Lipschitz function with constant  $L = \sqrt{\lambda_{\max}(\mathbf{K})}$ .

According to Proposition 2.5.2 and Theorem 5.2.2 in Papaspiliopoulos (2020), we have the following concentration inequality for a Lipschitz function of a standard Gaussian distribution:

$$\Pr(f(\mathbf{U}) \geq \mathbb{E}[f(\mathbf{U})] + t) \leq \exp\left(-\frac{t^2}{2L^2}\right).$$

Substituting  $f$  and  $L$ , we obtain

$$\Pr(\|\mathbf{Z} - \boldsymbol{\mu}\| \geq \mathbb{E}[\|\mathbf{Z} - \boldsymbol{\mu}\|] + t) \leq \exp\left(-\frac{t^2}{2\lambda_{\max}(\mathbf{K})}\right).$$

Since

$$\mathbb{E}[\|\mathbf{Z} - \boldsymbol{\mu}\|] \leq \sqrt{\mathbb{E}[\|\mathbf{Z} - \boldsymbol{\mu}\|^2]} = \sqrt{\text{tr}(\mathbf{K})},$$

we get the final result for a general Gaussian distribution:

$$\Pr(\|\mathbf{Z} - \boldsymbol{\mu}\| \geq \sqrt{\text{tr}(\mathbf{K})} + t) \leq \exp\left(-\frac{t^2}{2\lambda_{\max}(\mathbf{K})}\right). \quad (42)$$

Define the discrete set  $\mathcal{D}_M = \{\mathbf{x}_1, \dots, \mathbf{x}_M\} \subset \mathcal{X}$ . According to the above concentration inequality, we have

$$\Pr\left(\|\text{vec}(\mathbf{f}(\mathbf{x})) - \hat{\boldsymbol{\mu}}_n(\mathbf{x})\| > \sqrt{\text{tr}(\hat{\mathbf{K}}_n(\mathbf{x}, \mathbf{x}))} + z\right) \leq \exp\left(-\frac{z^2}{2\lambda_{\max}^{(n)}(\mathbf{x})}\right), \quad \forall \mathbf{x} \in \mathcal{D}_M,$$

where  $\lambda_{\max}^{(n)}(\mathbf{x})$  is the maximum eigenvalue of  $\hat{\mathbf{K}}_n(\mathbf{x}, \mathbf{x})$ .

By setting  $z = \sqrt{2\lambda_{\max}^{(n)}(\mathbf{x}) \log \frac{M}{\delta}}$ , we obtain

$$\Pr\left(\|\text{vec}(\mathbf{f}(\mathbf{x})) - \hat{\boldsymbol{\mu}}_n(\mathbf{x})\| \leq \beta_n \sqrt{\lambda_{\max}^{(n)}(\mathbf{x})}\right) \geq 1 - \delta, \quad \forall \mathbf{x} \in \mathcal{D}_M, \quad (43)$$

$$\text{where } \beta_n = \sqrt{\sup_{\mathbf{x} \in \mathcal{X}} \frac{\text{tr}(\hat{\mathbf{K}}_n(\mathbf{x}, \mathbf{x}))}{\lambda_{\max}^{(n)}(\mathbf{x})}} + \sqrt{2 \log \frac{M}{\delta}} = \sqrt{C_n} + \sqrt{2 \log \frac{M}{\delta}}.$$

From Lemma 1, we obtain that  $\|\text{vec}(\mathbf{f}(\mathbf{x})) - \text{vec}(\mathbf{f}(\mathbf{x}'))\| \leq (L' + C^\nabla) \|\mathbf{x} - \mathbf{x}'\|_1$  holds with probability at least  $1 - a \exp(-L'^2/b^2)$  for all  $\mathbf{x}, \mathbf{x}' \in \mathcal{X}$ .

Then, at round  $n$ , we set the size of  $\mathcal{D}_{M(n)}$  as  $(\tau_n)^d$ , i.e.,  $M(n) = (\tau_n)^d$ . For  $\mathbf{x} \in \mathcal{D}_{M(n)}$ , we have  $\|\mathbf{x} - [\mathbf{x}]_n\|_1 \leq \frac{rd}{\tau_n}$ , where  $[\mathbf{x}]_n$  is the closest point in  $\mathcal{D}_{M(n)}$  to  $\mathbf{x}$ .

Using the above aligns, if we set  $L' = b\sqrt{\log \frac{da}{\delta}}$ , we obtain

$$\|\text{vec}(\mathbf{f}(\mathbf{x})) - \text{vec}(\mathbf{f}([\mathbf{x}]_n))\| \leq \left(b\sqrt{\log \frac{da}{\delta}} + C^\nabla\right) \|\mathbf{x} - [\mathbf{x}]_n\|_1 \leq \left(b\sqrt{\log \frac{da}{\delta}} + C^\nabla\right) \frac{rd}{\tau_n},$$

with probability at least  $1 - \delta$  for all  $\mathbf{x} \in \mathcal{X}$ .

Choosing  $\tau_n = rd n^2 (b\sqrt{\log \frac{da}{\delta}} + C^\nabla)$ , we have

$$\Pr\left(\|\text{vec}(\mathbf{f}(\mathbf{x})) - \text{vec}(\mathbf{f}([\mathbf{x}]_M))\| \leq \frac{1}{n^2}\right) \geq 1 - \delta, \quad \forall \mathbf{x} \in \mathcal{X}.$$

Combining the above results, we obtain

$$\Pr\left(\|\text{vec}(\mathbf{f}(\mathbf{x}^*)) - \hat{\boldsymbol{\mu}}([\mathbf{x}^*]_n)\| \leq \beta_n \sqrt{\lambda_{\max}^{(n)}([\mathbf{x}^*]_n) + \frac{1}{n^2}}\right) \geq 1 - \delta,$$

where  $[\mathbf{x}^*]_n$  is the closest point in  $\mathcal{D}_{M(n)}$  to  $\mathbf{x}^*$ , and  $\beta_n = \sqrt{C_n} + 2d \log\left(\frac{rd n^2 (b\sqrt{\log(da/\delta)} + C^\nabla)}{\delta}\right)$ .

Part 2. Regret bound. According to the Lipschitz property of  $h$ , we have

$$r_n = h(\mathbf{x}^*) - h(\mathbf{x}_n) \leq L \|\text{vec}(\mathbf{f}(\mathbf{x}^*)) - \text{vec}(\mathbf{f}(\mathbf{x}_n))\|, \quad (44)$$

where  $L > 0$  is the Lipschitz constant.

Since

$$\hat{\boldsymbol{\mu}}_{n-1}(\mathbf{x}_n) + \beta_n \sqrt{\lambda_{\max}^{(n-1)}(\mathbf{x}_n)} \geq \hat{\boldsymbol{\mu}}_{n-1}([\mathbf{x}^*]_n) + \beta_n \sqrt{\lambda_{\max}^{(n-1)}([\mathbf{x}^*]_n)} \geq \text{vec}(\mathbf{f}(\mathbf{x}^*)) - \frac{1}{n^2},$$

we have

$$r_n \leq L \left( 2\beta_n \sqrt{\lambda_{\max}^{(n-1)}(\mathbf{x}_n)} + \frac{1}{n^2} \right). \quad (45)$$

We first consider the first term:

$$\begin{aligned} 4\beta_n^2 \lambda_{\max}^{(n-1)}(\mathbf{x}_n) &\leq 4\beta_N^2 \eta (\eta^{-1} \lambda_{\max}^{(n-1)}(\mathbf{x}_n)) \leq 4\beta_N^2 \eta C_2 \log(1 + \eta^{-1} \lambda_{\max}^{(n-1)}(\mathbf{x}_n)) \\ &\leq 4\beta_N^2 \eta C_2 \log |\mathbf{I}_T + \eta^{-1} \hat{\mathbf{K}}_{n-1}(\mathbf{x}_n, \mathbf{x}_n)|, \end{aligned}$$

where  $C_2$  is a constant.

Define  $C_1 = 4\eta C_2$ . Then

$$\sum_{n=1}^N 4\beta_n^2 \lambda_{\max}^{(n-1)}(\mathbf{x}_n) \leq C_1 N \beta_N^2 \sum_{n=1}^N \log |\mathbf{I}_T + \eta^{-1} \hat{\mathbf{K}}_{n-1}(\mathbf{x}_n, \mathbf{x}_n)| \leq C_1 N \beta_N^2 \gamma_N(\mathbf{K}, \eta),$$

where the last inequality holds by the definition of  $\gamma_N(\mathbf{K}, \eta)$ .

Since  $\sum_{n=1}^N \frac{1}{n^2} \leq \frac{\pi^2}{6}$ , we have the final result:

$$\sum_{n=1}^N r_n \leq L \left( \sqrt{C_1 N \gamma_N(\mathbf{K}, \eta)} \beta_N + \frac{\pi^2}{6} \right). \quad (46)$$

□

## H The proof of Proposition 2

Proof. We start from the definition of the (maximum) information gain:

$$\gamma_n(\mathbf{K}, \eta) = \max_{\mathbf{K}_n} \frac{1}{2} \log \det(\mathbf{I}_{nT} + \eta^{-1} \sigma^2 \mathbf{K}_n), \quad \mathbf{K}_n := [\mathbf{K}(\mathbf{x}_i, \mathbf{x}_j)]_{i,j=1}^n \in \mathbb{R}^{nT \times nT}. \quad (47)$$

Under the separable kernel in Definition 2, we have

$$\mathbf{K}(\mathbf{x}, \mathbf{x}') = (\text{vec}(\mathbf{A})\text{vec}(\mathbf{A})^\top) k(\mathbf{x}, \mathbf{x}') =: \mathbf{B} k(\mathbf{x}, \mathbf{x}'), \quad (48)$$

where  $\mathbf{B} := \text{vec}(\mathbf{A})\text{vec}(\mathbf{A})^\top \in \mathbb{R}^{T \times T}$ . Then, the Gram matrix factorizes as a Kronecker product

$$\mathbf{K}_n = \mathbf{K}_x \otimes \mathbf{B}, \quad \mathbf{K}_x = [k(\mathbf{x}_i, \mathbf{x}_j)]_{i,j=1}^n \in \mathbb{R}^{n \times n}. \quad (49)$$

Let  $\{\alpha_i\}_{i=1}^n$  be the eigenvalues of  $\mathbf{K}_x$  and  $\{\beta_j\}_{j=1}^T$  be the eigenvalues of  $\mathbf{B}$ . By the spectral property of the Kronecker product, the eigenvalues of  $\mathbf{K}_x \otimes \mathbf{B}$  are  $\{\alpha_i \beta_j : i = 1, \dots, n, j = 1, \dots, T\}$ . Therefore, we have

$$\log \det(\mathbf{I}_{nT} + \eta^{-1} \sigma^2 (\mathbf{K}_x \otimes \mathbf{B})) = \sum_{i=1}^n \sum_{j=1}^T \log(1 + c \alpha_i \beta_j), \quad c := \eta^{-1} \sigma^2. \quad (50)$$

For each fixed  $i$ , the function  $u \mapsto \log(1 + c \alpha_i u)$  is non-decreasing for  $u \geq 0$ , hence

$$\sum_{j=1}^T \log(1 + c \alpha_i \beta_j) = \sum_{j: \alpha_j > 0} \log(1 + c \alpha_i \beta_j) \leq T \cdot \log(1 + c \alpha_i \beta_{\max}), \quad (51)$$

where  $\beta_{\max} := \max_j \beta_j$ . Summing over  $i = 1, \dots, n$  and multiplying by  $1/2$  gives

$$\gamma_n(\mathbf{K}, \eta) \leq \frac{T}{2} \sum_{i=1}^n \log(1 + c \beta_{\max} \lambda_i) = T \cdot \gamma_n(k^\sharp, \eta), \quad (52)$$

where  $k^\sharp := \beta_{\max} k$  is simply a rescaled version of  $k$ . Since rescaling by a positive constant does not change the asymptotic order of the information gain, we obtain the general comparison bound

$$\gamma_n(\mathbf{K}, \eta) \leq T \cdot \gamma_n(k, \eta).$$

In our specific setting, the tightest bound is  $\gamma_n(\mathbf{K}, \eta) = \mathcal{O}(T \gamma_n(k, \eta))$ . Finally, we substitute known results for the scalar kernel  $k$ : (i) If  $k$  is the Gaussian (squared exponential) kernel in  $d$  dimensions, then  $\gamma_n(k, \eta) = \mathcal{O}((\log n)^{d+1})$ , which gives  $\gamma_n(\mathbf{K}, \eta) = \mathcal{O}(T(\log n)^{d+1})$ .

(ii) If  $k$  is a Matérn kernel with smoothness parameter  $\nu > 1$ , then  $\gamma_n(k, \eta) = \mathcal{O}(n^{\frac{d(d+1)}{2\nu+d(d+1)} \log n})$ , which gives  $\gamma_n(\mathbf{K}, \eta) = \mathcal{O}(T n^{\frac{d(d+1)}{2\nu+d(d+1)} \log n})$ .  $\square$

## I The proof of Theorem 2

Denote  $\tilde{h}(\mathbf{x}, \boldsymbol{\lambda}) = H_f \tilde{\mathbf{f}}(\mathbf{x}, \boldsymbol{\lambda})$ , then we have

$$\begin{aligned} \tilde{h}(\mathbf{x}^*, \boldsymbol{\lambda}^*) - \tilde{h}(\mathbf{x}_n, \boldsymbol{\lambda}_n) &= \left[ \tilde{h}(\mathbf{x}^*, \boldsymbol{\lambda}^*) - \tilde{h}(\mathbf{x}_n, \boldsymbol{\lambda}^*) \right] + \left[ \tilde{h}(\mathbf{x}_n, \boldsymbol{\lambda}^*) - \tilde{h}(\mathbf{x}_n, \boldsymbol{\lambda}_n) \right] \\ &= r_{1n} + r_{2n}. \end{aligned}$$

For the first item, according to the Cauchy-Schwarz inequality, we have

$$H_f \tilde{\mathbf{f}}(\mathbf{x}, \boldsymbol{\lambda}) - H_f \tilde{\boldsymbol{\mu}}_n(\mathbf{x}, \boldsymbol{\lambda}) \leq H \|\tilde{\mathbf{f}}(\mathbf{x}, \boldsymbol{\lambda}) - \tilde{\boldsymbol{\mu}}_n(\mathbf{x}, \boldsymbol{\lambda})\|. \quad (53)$$

Similar to the proof of Theorem 1, we provide the following lemma.

Lemma 2. Under Assumption 1-3, suppose the noise vectors  $\{\text{vec}(\boldsymbol{\varepsilon}_i)\}_{i \geq 1}$  are independently and identically distributed in  $N(0, \sigma^2 \mathbf{I}_k)$ . Then, for any  $\delta \in (0, 1]$ , with probability at least  $1 - \delta$ ,  $\|\tilde{\mathbf{f}}(\mathbf{x}, \boldsymbol{\lambda}) - \tilde{\boldsymbol{\mu}}_n(\mathbf{x}, \boldsymbol{\lambda})\|_2 \leq \beta_n \|\tilde{\mathbf{K}}_n(\mathbf{x}, \mathbf{x}; \boldsymbol{\lambda}, \boldsymbol{\lambda})\|^{1/2}$  holds uniformly over all  $\mathbf{x} \in \mathcal{X}$  and  $\boldsymbol{\lambda} \in \Lambda$  and  $i \geq 1$ , where  $\beta_n = \sqrt{\tilde{C}_n + 2d \log(\frac{rdn^2(b\sqrt{\log(da/\delta)} + \tilde{C}_\nabla)}{l})\delta}$ ,  $\tilde{C}_n = \sup_{\mathbf{x} \in \mathcal{X}} \frac{\text{tr}(\tilde{\mathbf{K}}_n(\mathbf{x}, \mathbf{x}; \boldsymbol{\lambda}_n^*, \boldsymbol{\lambda}_n^*))}{\lambda_{\max}^{(n)}(\mathbf{x}, \boldsymbol{\lambda}_n^*)}$ , and  $\tilde{C}_\nabla = \sup_{\mathbf{x} \in \mathcal{X}} \sqrt{\text{tr}(\tilde{\mathbf{K}}_n^\nabla(x_j, x_j))}$ .

From Lemma 2 and (53), we have

$$H_f \tilde{\mathbf{f}}(\mathbf{x}, \boldsymbol{\lambda}) - H_f \tilde{\boldsymbol{\mu}}_n(\mathbf{x}, \boldsymbol{\lambda}) \leq H \|\tilde{\mathbf{f}}(\mathbf{x}, \boldsymbol{\lambda}) - \tilde{\boldsymbol{\mu}}_n(\mathbf{x}, \boldsymbol{\lambda})\| \leq H \beta_n \|\tilde{\mathbf{K}}_n(\mathbf{x}, \mathbf{x}; \boldsymbol{\lambda}, \boldsymbol{\lambda})\|^{1/2}.$$

Then, we have

$$\begin{aligned} r_{1n} &= \tilde{h}(\mathbf{x}^*, \boldsymbol{\lambda}^*) - \tilde{h}(\mathbf{x}_n, \boldsymbol{\lambda}^*) \\ &\leq H_f(\tilde{\boldsymbol{\mu}}_n(\mathbf{x}^*, \boldsymbol{\lambda}^*)) + H \tilde{\beta}_n \|\tilde{\mathbf{K}}_{n-1}(\mathbf{x}^*, \mathbf{x}^*)\|^{1/2} - H_f(\tilde{\mathbf{f}}(\mathbf{x}_n, \boldsymbol{\lambda}^*)) \\ &\leq 2H \tilde{\beta}_{n-1} \|\tilde{\mathbf{K}}_{n-1}(\mathbf{x}_n, \mathbf{x}_n; \boldsymbol{\lambda}^*, \boldsymbol{\lambda}^*)\|^{1/2}. \end{aligned}$$

Similar to Theorem 1, we obtain

$$\begin{aligned} R_{1N} &:= \sum_{n=1}^N r_{1n} \leq 2H \tilde{\beta}_{n-1} \|\tilde{\mathbf{K}}_{n-1}(\mathbf{x}_n, \mathbf{x}_n; \boldsymbol{\lambda}^*, \boldsymbol{\lambda}^*)\|^{1/2} \\ &\leq H \left( \sqrt{C_3 N \gamma_N(\tilde{\mathbf{K}}, \eta)} \tilde{\beta}_N + \frac{\pi^2}{6} \right), \end{aligned}$$

where  $C_3 > 0$  is a constant.

For the second item, followed in Accabi et al. (2018), we have

$$R_{2N} \leq H \sqrt{C_4 T N \tilde{\gamma}_N(\tilde{\mathbf{K}}, \eta)} \tilde{\rho}_N,$$

where  $C_4 > 0$  is a constant.

Then we have the cumulative regret over  $N$  rounds is bounded by

$$\begin{aligned} r_n &\leq r_{1n} + r_{2n} \\ &\leq H \left( \sqrt{C_3 \gamma_N(\tilde{\mathbf{K}}, \eta) N} \tilde{\beta}_N + \frac{\pi^2}{6} + \sqrt{C_4 T N \tilde{\gamma}_N(\tilde{\mathbf{K}}, \eta)} \tilde{\rho}_N \right). \end{aligned}$$

## J The proof of Proposition 3

Proof. Based on the definition of the (maximum) information gain, we have

$$\gamma_n(\tilde{\mathbf{K}}, \eta) = \max_{\mathbf{X}_n} \frac{1}{2} \log \det(\mathbf{I}_m + c \tilde{\mathbf{K}}_n), \quad c := \eta^{-1} \sigma^2, \quad (54)$$

where the Gram matrix takes the form  $\tilde{\mathbf{K}}_n = \mathbf{E} \mathbf{K}_n \mathbf{E}^\top$  and  $\mathbf{K}_n = \mathbf{B} \otimes \mathbf{K}_x$ , with  $\mathbf{K}_x = [k(\mathbf{x}_i, \mathbf{x}_j)]_{i,j=1}^n \in \mathbb{R}^{n \times n}$ ,  $\mathbf{B} = \text{vec}(\mathbf{A}) \text{vec}(\mathbf{A})^\top \in \mathbb{R}^{T \times T}$ .

By Sylvester's identity, we have

$$\det(\mathbf{I}_{nk} + c \mathbf{E}_n \mathbf{K}_n \mathbf{E}_n^\top) = \det(\mathbf{I}_{nT} + c \mathbf{K}_n^{1/2} \mathbf{E}_n^\top \mathbf{E}_n \mathbf{K}_n^{1/2}). \quad (55)$$

Since  $\mathbf{E}_n$  selects rows,  $0 \preceq \mathbf{E}_n^\top \mathbf{E}_n \preceq \mathbf{I}_{nT}$ , hence

$$\begin{aligned} \log \det(\mathbf{I}_{nk} + c \mathbf{E}_n \mathbf{K}_n \mathbf{E}_n^\top) &= \log \det(\mathbf{I}_{nT} + c \mathbf{K}_n^{1/2} \mathbf{E}_n^\top \mathbf{E}_n \mathbf{K}_n^{1/2}) \\ &\leq \log \det(\mathbf{I}_{nT} + c \mathbf{K}_n). \end{aligned} \quad (56)$$

Then, followed in Proposition 1, we have

$$\gamma_n(\tilde{\mathbf{K}}_n, \eta) = \mathcal{O}(T(\log n)^{d+1}) \text{ for the Gaussian kernel,} \quad (57)$$

$$\gamma_n(\tilde{\mathbf{K}}_n, \eta) = \mathcal{O}\left(T n^{\frac{d(d+1)}{2\nu+d(d+1)}} \log n\right) \text{ for the Matérn kernel.} \quad (58)$$

From (56), we also obtain that

$$\tilde{\gamma}_n(\tilde{\mathbf{K}}_n, \eta) = \mathcal{O}(T(\log n)^{d+1}) \text{ for the Gaussian kernel,} \quad (59)$$

$$\tilde{\gamma}_n(\tilde{\mathbf{K}}_n, \eta) = \mathcal{O}\left(Tn^{\frac{d(d+1)}{2\nu+d(d+1)}} \log n\right) \text{ for the Matérn kernel.} \quad (60)$$

□

## K Detailed settings of the experiments

### K.1 Detailed settings of synthetic experiments

The setting of simulations are as follows:

- Compute resources: All experiments were run on a Windows 10 Pro (Build 19045) desktop with an Intel Core i9-7900X CPU (3.10 GHz) and 32 GB RAM.
- Kernel setting: We use the Matérn kernel function with the smoothing parameter  $\nu = 5/2$  as the input kernel for different GPs.
- Data setting: For the GP prediction, we generate  $n_{train} = 10d$  training samples for estimating hyperparameters and  $n_{test} = 5d$  testing samples for predicting. In the BO and CBBO framework, we generate  $n_0 = 5d$  initial design points based on Latin Hypercube Sampling (LHS), and  $N = 10d$  sequential design points.
- Criteria: To compare the GPs prediction performance of different methods, we use the following criteria:
  - (1) Negative Log-Likelihood (NLL): It measures how well a probabilistic model fits the observed data. For given data  $\mathbf{X}_n$  and  $\mathbf{Y}_n$ , the NLL is defined as  $\text{NLL} = \frac{1}{2} \log(\tau^2 \mathbf{K}_n + \sigma^2 \mathbf{I}_{nT}) + \frac{1}{2} \mathbf{Y}_n^\top (\tau^2 \mathbf{K}_n + \sigma^2 \mathbf{I}_{nT})^{-1} \mathbf{Y}_n$ .
  - (2) Mean Absolute Error (MAE):  $\text{MAE} = \frac{1}{n_{test}} \sum_{i=1}^{n_{test}} \frac{\|\mathbf{y}_i - \hat{\mathbf{y}}_i\|}{\|\mathbf{y}_i\|}$ .
  - (3) Covariance Operator Norm ( $\|Cov\|$ ):  $\|\hat{\mathbf{K}}_n\| = \sup_{\|\mathbf{v}\|=1} \|\hat{\mathbf{K}}_n \mathbf{v}\|$ .

For the BO framework, we use the the mean squared error of inputs ( $\text{MSE}_x$ ) and the mean absolute error of outputs  $\text{MAE}_y$  to compare the optimization performance of different methods. Here  $\text{MSE}_x = \|\mathbf{x}^* - \mathbf{x}_N^*\|^2$ , and  $\text{MAE}_y = \|\frac{\mathbf{f}^* - \mathbf{f}_N}{\mathbf{f}^*}\|$  over  $N$  rounds. For the CBBO framework, we add the Acc criterion to compare the match between the optimal super arm and the super arm chosen over  $N$  rounds, that is,  $\text{Acc} = \mathbb{I}_{\mathbf{x}^* = \mathbf{x}_N}/k$ , where  $\mathbb{I}$  is a indictor function.

### K.2 Detailed settings of case studies

The detailed datasets of case studies are as follows:

**Chemistry reaction (CHEM):** Reaction optimization is fundamental to synthetic chemistry, from improving yields in industrial processes to selecting reaction conditions for drug candidate synthesis. According to Shields et al. (2021), we aim to evaluate the reaction parameters ( $x_1$ : concentration,  $x_2$ : temperature) to improve the experimental yields ( $\mathbf{y} : 4 \times 3 \times 3$ ) of palladium-catalysed direct arylation reaction under varying bases (Mode 1), ligands (Mode 2), and solvents (Mode 3).

**PS/PAN material (MAT):** Electrospun polystyrene/polyacrylonitrile (PS/PAN) materials are commonly used as potential oil sorbents for marine oil spill remediation. From Wang et al. (2020), we aim to optimize the fabrication parameters of PS/PAN materials, including spinneret speed ( $x_1$ ), collector distance ( $x_2$ ), applied voltage ( $x_3$ ), and fiber diameter ( $x_4$ ), to improve their oil absorption capacity ( $\mathbf{y} : 5 \times 4 \times 4$ ) under varying PS content (Mode 1), mass fraction (Mode 2), and  $\text{SiO}_2$  content (Mode 3).

**3D printing (PRINT):** Material extrusion-based three-dimensional printed products have been widely used in aerospace, automotive, and other fields. Following Zhai et al. (2023), we focus on selecting appropriate process parameters ( $x_1$ : layer thickness,  $x_2$ : platform temperature,  $x_3$ : nozzle temperature,  $x_4$ : infill density, and  $x_5$ : printing speed) to reduce

variations in part quality ( $\mathbf{y} : 3 \times 4 \times 3$ ) caused by different printer nozzles (Mode 1) and printing geometries (Mode 2). The quality (Mode 3) is evaluated in terms of compression deformation, compressive strength, and the printing cost.

Renewable energy (REEN): Climate change affects the availability and reliability of renewable energy sources such as wind, solar, and hydropower. We employ the operational energy dataset from the Copernicus Climate Change Service (<https://cds.climate.copernicus.eu/datasets/sis-energy-derived-reanalysis?tab=overview>) to explore the climate conditions that are most beneficial to renewable energy generation in various European nations. The climate-related variables, used as input features, include air temperature ( $x_1$ ), precipitation ( $x_2$ ), surface incoming solar radiation ( $x_3$ ), wind speed at 10 meters ( $x_4$ ) and 100 meters ( $x_5$ ), and mean sea level pressure ( $x_6$ ). The energy-related indicators ( $\mathbf{y} : 10 \times 2$ ) collected from ten European countries (Mode 1), used as outputs, include the capacity factor ratio of solar photovoltaic power generation and wind power generation onshore (Mode 2).

## L The comparison of computational complexity for baselines

To provide a clearer comparison, we summarize the computational complexity of GP training, BO, and CBBO for the baseline methods sMTGP, MLGP, and MVGP, together with our proposed method, in the table below. Here  $m_h$ ,  $m_{h1}$ ,  $m_{h2}$ , and  $m_{hl}$  for  $l = 1, \dots, m$

Table 5: The computational complexity of different methods for GP training, BO, and CBBO.

Task	Method	Computational complexity
GP Training	TOGP	$\mathcal{O}((n^3T^3 + n^2T^2m_h)\log n)$
	sMTGP	$\mathcal{O}((n^3 + \sum_{l=1}^m t_l^3 + n^2m_h + \sum_{l=1}^m t_l^2m_{hl})\log n)$
	MLGP	$\mathcal{O}((n^3 + \sum_{l=1}^m t_l^3 + n^2m_h + \sum_{l=1}^m t_l^2m_{hl})\log n)$
	MVGP	$\mathcal{O}((n^3 + T^3 + n^2m_{h1} + T^2m_{h2})\log n)$
BO (Round $n$ )	TOGP	$\mathcal{O}((n^3T^3 + n^2T^2m_h)\log n)$
	sMTGP	$\mathcal{O}((n^3 + \sum_{l=1}^m t_l^3 + n^2m_h + \sum_{l=1}^m t_l^2m_{hl})\log n)$
	MLGP	$\mathcal{O}((n^3 + \sum_{l=1}^m t_l^3 + n^2m_h + \sum_{l=1}^m t_l^2m_{hl})\log n)$
	MVGP	$\mathcal{O}((n^3 + T^3 + n^2m_{h1} + T^2m_{h2})\log n)$
CBBO (Round $n$ )	TOGP	$\mathcal{O}((n^3k^3 + n^2kTm_h)\log n + kT^3)$
	sMTGP	$\mathcal{O}((n^3 + k^3 + n^2m_h + k \sum_{l=1}^m t_l m_{hl})\log n + k \sum_{l=1}^m t_l^3)$
	MLGP	$\mathcal{O}((n^3 + k^3 + n^2m_h + k \sum_{l=1}^m t_l m_{hl})\log n + k \sum_{l=1}^m t_l^3)$
	MVGP	$\mathcal{O}((n^3 + T^3 + n^2m_{h1} + kTm_{h2})\log n + kT^3)$

denote the numbers of hyperparameters for the corresponding methods.

Furthermore, we report the empirical computational time for GP training across all methods under the three experimental settings. The results are summarized below.

Table 6: The runtime (s) of different methods for GP training in the three synthetic settings.

	TOGP	sMTGP	MLGP	MVGP
Setting (1)	266.04	27.26	30.57	6.50
Setting (2)	69.85	16.08	21.99	1.31
Setting (3)	900.13	851.34	891.73	769.50

We further report the empirical running time of BO and CBBO under all baseline methods. The results are summarized in the table below.

Finally, we provide the prediction and optimization performance of TOGP based on the Nyström low-rank approximation (SVD-TOGP) in Remark 3 under the three synthetic settings. The results are summarized below.

Table 7: The runtime (s) of different methods for BO and CBBO in the three synthetic settings.

Method/Task	Setting (1)		Setting (2)		Setting (3)	
	BO	CBBO	BO	CBBO	BO	CBBO
TOBO/TOCBBO	6968.25	8017.08	1588.53	2348.16	6035.61	11699.09
sMTGP-UCB	1516.31	953.82	117.78	179.11	5291.26	9436.90
MLGP-UCB	1545.41	981.86	133.93	185.49	5452.90	9696.60
MVGP-UCB	340.44	437.29	14.86	20.76	3006.97	3199.47
TOGP-RS	6176.84	7990.44	1573.36	2338.97	5786.02	11501.01
sMTGP-RS	1503.24	939.27	106.93	164.95	5273.84	9421.08
MLGP-RS	1530.32	971.25	109.14	180.70	5252.32	9431.96
MVGP-RS	334.79	386.86	7.70	6.70	2997.75	3116.23

Task	Criterion	Setting (1)		Setting (2)		Setting (3)	
		SVD-TOGP	TOGP	SVD-TOG	TOGP	SVD-TOGP	TOGP
GP Training	NLL	557.09	503.00	-18.39	-18.10	-3778.74	-3923.10
	MAE	0.1756	0.1571	0.1099	0.1052	0.1436	0.1372
	$\ Cov\ $	3.9627	2.0200	0.6261	0.0400	0.0881	2.8200
	Time (s)	21.80	266.04	10.83	69.85	436.17	900.13
BO	$MSE_x$	0.0001	0.0000	0.0003	0.0003	0.0002	0.0001
	$MAE_y$	0.0041	0.0008	0.0356	0.0350	0.0051	0.0050
	Ins Regret	0.0040	0.0001	0.0002	0.0002	0.0402	0.0302
	Time (s)	831.02	6968.25	162.78	1588.53	3604.66	6035.61
CBBO	$MSE_x$	0.0024	0.0023	0.0000	0.0000	0.0035	0.0021
	$MAE_y$	0.0180	0.0172	0.0000	0.0000	0.0246	0.0145
	Acc	1	1	1	1	1	1
	Ins Regret	1.0944	0.9807	0.0000	0.0000	1.8571	1.4406
	Time (s)	655.83	8017.08	134.22	2348.16	4446.12	11699.09

## M Additional results of Synthetic Experiments

Table 8: The additional optimization performance of different methods in three synthetic settings.

k	Setting (1)			Setting (2)			Setting (3)			
	MSE <sub>x</sub>	MAE <sub>y</sub>	Acc	MSE <sub>x</sub>	MAE <sub>y</sub>	Acc	MSE <sub>x</sub>	MAE <sub>y</sub>	Acc	
T/3	TOCBBO	0.0054	0.0509	1.00	0.0001	0.0036	1.00	0.0021	0.0312	1.00
	SMTGP-UCB	0.0057	0.0942	1.00	0.0548	0.3336	1.00	0.0340	0.8616	0.71
	MLGP-UCB	0.0677	0.9775	0.33	0.0434	0.6961	0.50	0.3549	0.8205	0.29
	MVGP-UCB	0.0325	0.7530	0.33	0.0019	0.0191	1.00	0.0405	0.3647	0.71
	TOGP-RS	0.0208	1.3279	0.83	0.0206	0.4347	0.50	0.0709	1.5521	0.57
	SMTGP-RS	0.0203	1.2625	0.50	0.1201	0.4443	0.50	0.0254	1.0703	0.50
	MLGP-RS	0.0619	1.0296	0.67	0.1191	0.5081	1.00	0.1816	1.1735	0.64
	MVGP-RS	0.0634	0.9733	0.67	0.0469	0.4444	0.50	0.0574	1.3837	0.43
2T/3	TOCBBO	0.0006	0.0125	1.00	0.0010	0.0076	1.00	0.0103	0.1163	0.96
	SMTGP-UCB	0.0066	0.0585	1.00	0.0012	0.0177	1.00	0.0122	1.9890	0.89
	MLGP-UCB	0.0323	3.6747	0.82	0.2229	1.4532	0.75	0.0423	4.0294	0.81
	MVGP-UCB	0.0047	0.4765	1.00	0.0022	0.0309	1.00	0.0324	1.4985	0.93
	TOGP-RS	0.0128	4.6512	0.82	0.0202	1.1872	1.00	0.0218	10.4919	0.70
	SMTGP-RS	0.0128	4.6512	0.82	0.2229	1.4532	0.75	0.0110	6.0795	0.70
	MLGP-RS	0.0323	3.6747	0.82	0.2229	1.4532	0.75	0.0423	4.0294	0.81
	MVGP-RS	0.0128	4.6512	0.82	0.0439	0.8309	1.00	0.0423	4.0294	0.81

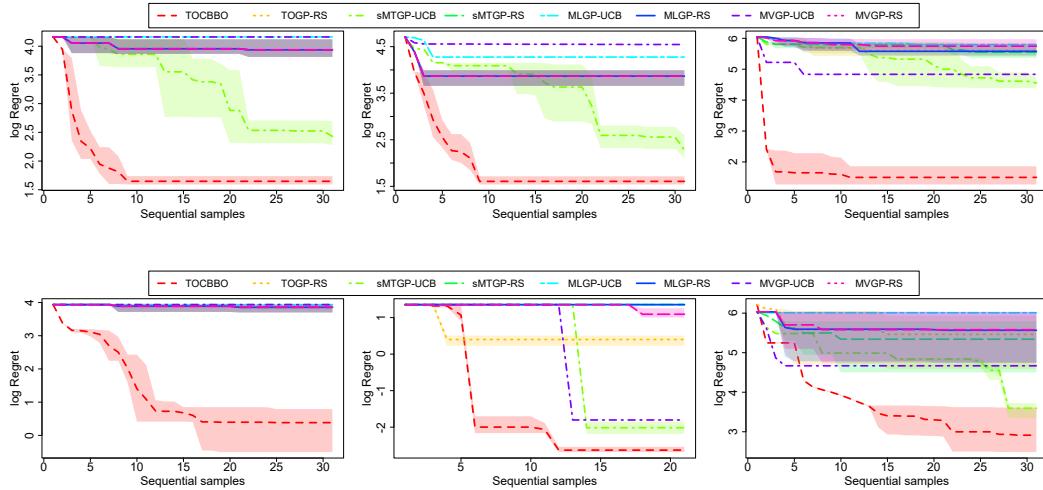


Figure 4: Each round’s logarithmic instantaneous regret of different methods in the Setting (1) (Left), (2) (Middle), and (3) (Right) when  $k = T/3$  (Top row) and  $k = 2T/3$  (Bottom row).

Table 9: Summary across CHEM, MAT, and PRINT datasets with 10 repetitions.

Method	CHEM	MAT	PRINT
TOBO	100 (0.00)	150.07 (0.00)	-25.03 (0.00)
sMTGP-UCB	99.91 (0.10)	147.97 (2.24)	-25.03 (0.00)
MLGP-UCB	99.29 (0.75)	147.90 (2.32)	-25.13 (0.11)
MVGP-UCB	96.32 (4.89)	147.20 (3.44)	-25.27 (0.32)
TOGP-RS	93.84 (1.56)	147.83 (2.32)	-25.27 (0.23)
sMTGP-RS	96.63 (3.74)	146.22 (4.30)	-25.03 (0.13)
MLGP-RS	99.41 (0.76)	148.28 (1.64)	-25.27 (0.23)
MVGP-RS	96.32 (3.72)	147.20 (2.80)	-25.27 (0.33)

In the BO setting, we additionally include a single-objective GP-UCB baseline, which directly assumes that  $L_f \mathbf{f}$  follows a GP and uses the UCB acquisition function to select query points sequentially. The optimization results under the three settings in our numerical experiments are summarized below.

Table 10: The results of Single GP-UCB in three synthetic settings.

	Criterion	Single GP-UCB	TOBO
Setting (1)	$MSE_x$	0.0004	0.0000
	Ins Regret	0.0459	0.0001
	Time	457.34	6968.25
Setting (2)	$MSE_x$	0.4761	0.0003
	Ins Regret	0.2093	0.0002
	Time	187.30	1588.53
Setting (3)	$MSE_x$	0.0084	0.0001
	Ins Regret	0.1964	0.0302
	Time	415.61	6035.61

We include an independent GP-UCB baseline (Ind GP-UCB), which assumes that each tensor element follows its own GP model and applies the proposed CMAB-UCB2 acquisition function to sequentially select both query points and super-arms. The optimization results under the three synthetic settings are summarized below.

Table 11: The results of the Ind GP-UCB in three synthetic settings.

	Criterion	Ind GP-UCB	TOBO
Setting (1)	$MSE_x$	0.2121	0.0023
	$MAE_y$	0.6739	0.0172
	Acc	0.67	1
	Ins Regret	36.301	0.9807
	Time (s)	328.56	8017.08
Setting (2)	$MSE_x$	0.0731	0.0000
	$MAE_y$	0.0486	0.0000
	Acc	1	1
	Ins Regret	0.1561	0.0000
	Time (s)	110.77	2348.16
Setting (3)	$MAE_y$	0.0139	0.0021
	Acc	0.86	1
	Ins Regret	54.2714	1.4406
	Time (s)	3296.72	11699.09

For non-separable multi-output GPs (Fricker et al., 2013), we additionally provide the results under the three synthetic settings below.

As shown, TOBO achieves consistently better optimization accuracy than Single GP-UCB, Ind GP-UCB, and non-separable MOGP-UCB across all settings. Although the runtime of TOBO is higher, we further introduce an efficient variant named SVD-TOBO, which employs a low-rank eigen-decomposition to approximate the TOGP covariance in Remark 3 and significantly reduces runtime.

To evaluate the sensitivity of our method with respect to different choices of  $L_f$  and  $H_f$ , we consider three types of operators defined as follows (Chugh, 2020).

- Sum operator (used in the main manuscript):

$$L_f \mathbf{f}(\mathbf{x}) = \sum f_{i_1, \dots, i_m}(\mathbf{x}), \quad H_f \tilde{\mathbf{f}}(\mathbf{x}, \boldsymbol{\lambda}) = \sum \tilde{f}_{i_1, \dots, i_m}(\mathbf{x}, \boldsymbol{\lambda}).$$

Table 12: The results of the non-separable MOGP in three synthetic settings.

Task	Criterion	Setting (1)	Setting (2)	Setting (3)
GP	NLL	507.19	-39.33	-3094.10
	MAE	0.1923	0.1493	0.1591
	$\ \text{Cov}\ $	6.7398	0.5618	20.5800
	Time (s)	453.11	151.31	1397.68
BO	$\text{MSE}_x$	0.0014	0.0005	0.0244
	$\text{MAE}_y$	0.0536	0.0503	0.6277
	Ins Regret	1.0284	0.0030	6.6283
	Time (s)	9109.08	2101.45	7881.31
CBBO	$\text{MSE}_x$	0.0073	0.0683	0.0091
	$\text{MAE}_y$	0.0643	0.0390	0.1257
	Acc	1	1	0.86
	Ins Regret	1.7389	0.1551	51.4646
	Time (s)	10462.18	3107.82	14175.50

- Weighted sum operator:

$$L_f \mathbf{f}(\mathbf{x}) = \sum w_{i_1, \dots, i_m} f_{i_1, \dots, i_m}(\mathbf{x}), \quad H_f \tilde{\mathbf{f}}(\mathbf{x}, \boldsymbol{\lambda}) = \sum w_{i_1, \dots, i_m} \tilde{f}_{i_1, \dots, i_m}(\mathbf{x}, \boldsymbol{\lambda}),$$

where  $w_{i_1, \dots, i_m} \sim U(0, 1)$ .

- Exponential weighted operator:

$$L_f \mathbf{f}(\mathbf{x}) = \sum e^{p w_{i_1, \dots, i_m} - 1} e^{p f_{i_1, \dots, i_m}(\mathbf{x})}, \quad H_f \tilde{\mathbf{f}}(\mathbf{x}, \boldsymbol{\lambda}) = \sum e^{p w_{i_1, \dots, i_m} - 1} e^{p \tilde{f}_{i_1, \dots, i_m}(\mathbf{x}, \boldsymbol{\lambda})},$$

where  $p = 2$  and  $w_{i_1, \dots, i_m} \sim U(0, 1)$ .

The results under Setting (1) in our numerical experiments are summarized below. It can

Table 13: The results of different operators in three synthetic settings.

	Criterion	Sum operator	Weighted sum operator	Exponential weighted operator
BO	$\text{MSE}_x$	0.0000	0.0000	0.0000
	$\text{MAE}_y$	0.0008	0.0083	0.0072
	Ins Regret	0.0001	0.0044	0.0533
CBBO	$\text{MSE}_x$	0.0023	0.0037	0.0025
	$\text{MAE}_y$	0.0172	0.0329	0.0548
	Acc	1	1	1
	Ins Regret	0.1964	0.0107	0.4972

be seen that our method is robust across different choices of  $L_f$  and  $H_f$ , and both TOBO and TOCBBO consistently achieve strong optimization performance.

## N Real-world Application: Semiconductor manufacturing process

A motivating example arises from semiconductor manufacturing, where each wafer consists of numerous dies (chips) arranged in a two-dimensional grid. During the Chip Probing (CP) phase, a critical stage for functional quality control, each die is evaluated based on multiple quality variables such as voltage, current, leakage, and power consumption. These variables are spatially correlated across neighboring dies due to physical effects such as process variation and mechanical stress, forming a naturally structured tensor output. To ensure high yield and reliability, manufacturers aim to adjust process control parameters (inputs) so that all quality variables across the wafer remain within target specifications. This leads to an optimization problem where the output is a three-mode tensor: the first two

modes index the die positions on the wafer, and the third mode captures multiple quality variables. Such a scenario cannot be effectively modeled by scalar- or vector-output BO approaches, as they would lose essential structural information.

In practice, each wafer may contain hundreds of dies. However, resource and time constraints often make it infeasible to measure all quality variables across all die positions on every wafer. Manufacturers instead selectively measure a subset of output entries, such as centrally located dies, those more prone to failure, or historically most informative regions. Similarly, only a subset of quality variables may be measured if certain tests are time-consuming or costly. This results in a partially observed tensor, where only part of the full output is available at each iteration.

We incorporate this example into the revised paper and conduct a corresponding case study. The input is  $\mathbf{x} = (x_1, x_2, x_3)$  representing process parameters, and the output  $\mathbf{f}(\mathbf{x}) \in \mathbb{R}^{5 \times 5 \times 3}$  denotes die-wise quality variables on the wafer. A black-box semiconductor simulator is employed as the true system. We generate 5 observations as the initial design and then sequentially select 20 queried points based on different BO methods. Tables 14 and 15 compare the performance of TOBO and TOCBBO against several baselines. Our methods significantly outperform the alternatives in terms of input accuracy ( $MAE_x$ ), regret, and final objective value, demonstrating their superiority.

	TOBO	sMTGP-UCB	MLGP-UCB	MVGP-UCB
$MAE_x$	0.0651 (0.0016)	0.1997 (0.0020)	0.1579 (0.0059)	0.2669 (0.0046)
Regret	0.1702 (0.0007)	0.2400 (0.0014)	0.1956 (0.0088)	0.3818 (0.0029)
Objective	0.8298 (0.0009)	0.7600 (0.0031)	0.8044 (0.0079)	0.6182 (0.0033)

Table 14: Performance comparison of TOBO with baseline methods in terms of  $MAE_x$ , regret, and objective (mean and standard deviation).

	TOCBBO	sMTGP-UCB	MLGP-UCB	MVGP-UCB
$MAE_x$	0.1453 (0.0466)	0.4313 (0.0592)	0.5702 (0.0747)	0.6758 (0.0844)
Regret	0.1431 (0.0388)	0.2483 (0.0522)	0.4338 (0.0918)	0.3461 (0.0709)
Objective	0.6085 (0.0436)	0.5290 (0.0500)	0.4282 (0.1147)	0.4794 (0.0912)

Table 15: Performance comparison of TOCBBO with baseline methods in terms of  $MAE_x$ , regret, and objective (mean and standard deviation).

These results show that the proposed methods can effectively optimize under partially observed tensor data, highlighting their practical relevance for semiconductor manufacturing.